

The Hintermann–Merlini–Baxter–Wu and the Infinite-Coupling-Limit Ashkin–Teller Models

Yuan Huang

*Hefei National Laboratory for Physical Sciences at Microscale
and Department of Modern Physics
University of Science and Technology of China
Hefei, Anhui 230026, CHINA
HUANGY22@MAIL.USTC.EDU.CN*

Youjin Deng

*Hefei National Laboratory for Physical Sciences at Microscale
and Department of Modern Physics
University of Science and Technology of China
Hefei, Anhui 230026, CHINA
YJDENG@USTC.EDU.CN*

Jesper Lykke Jacobsen

*Laboratoire de Physique Théorique
École Normale Supérieure
24 rue Lhomond
75231 Paris, FRANCE
and
Université Pierre et Marie Curie
4 place Jussieu
75252 Paris, FRANCE
JACOBSEN@LPT.ENS.FR*

Jesús Salas

*Grupo de Modelización, Simulación Numérica y Matemática Industrial
Universidad Carlos III de Madrid
Avda. de la Universidad, 30
28911 Leganés, SPAIN
and
Grupo de Teorías de Campos y Física Estadística
Instituto Gregorio Millán, Universidad Carlos III de Madrid
Unidad Asociada al IEM-CSIC
Madrid, SPAIN
JSALAS@MATH.UC3M.ES*

October 9, 2012
Revised November 19, 2012

Abstract

We show how the Hintermann–Merlini–Baxter–Wu model (which is a generalization of the well-known Baxter–Wu model to a general Eulerian triangulation) can be mapped onto a particular infinite-coupling-limit of the Ashkin–Teller model. We work out some mappings among these models, also including the standard and mixed Ashkin–Teller models. Finally, we compute the phase diagram of the infinite-coupling-limit Ashkin–Teller model on the square, triangular, hexagonal, and kagome lattices.

Key Words: Baxter–Wu model; Ashkin–Teller model; Hintermann–Merlini–Baxter–Wu model; Infinite-coupling-limit Ashkin–Teller model; partial trace transformation; plane Eulerian triangulation.

1 Introduction

In 1944 Onsager [1] solved the nearest-neighbor square-lattice Ising model without magnetic field. This constitutes a major milestone in Statistical Mechanics. This achievement opened the door to find other exactly two-dimensional solvable models using different approaches. Two of such lines of research were (1) to consider models with multi-spin interactions rather than nearest-neighbor couplings, and (2) to look for models with larger symmetry groups than \mathbb{Z}_2 .

Two different groups obtained positive results along the first line of research using 3-spin interactions. In particular, in 1972 Hintermann and Merlini [2] solved the Ising model with 3-spin interactions on the union-jack lattice. They use a mapping of this model onto the 8-vertex model [3], and used Baxter’s solution of the latter [3] (another milestone in Statistical Mechanics) to derive the critical points of the model. Soon after this result, Baxter and Wu [4, 5] found in 1973 the exact solution of an Ising model on a triangular lattice also with pure 3-spin interactions. The method chosen was the Bethe Ansatz [3]. This model is very interesting, as it is believed [6] to belong to the same universality class as the 4-state Potts model [3, 7], but it does not show the logarithmic corrections displayed by the latter model [8–10]. The field theoretical interpretation of these differing behaviors is the following. The dominant part of the action describing the continuum limit of both the 4-state Potts model and the Baxter-Wu model is that of a free bosonic field. Both models contain further strictly irrelevant operators, which are not necessarily identical, since they may depend on the discrete symmetries of the spins and of the lattices on which the models are defined. But crucially, the 4-state Potts model contains in addition a marginally irrelevant operator, which is not present in the Baxter-Wu model. This latter operator induces logarithmic corrections under the renormalization-group flow that takes the 4-state Potts model to the fixed-point theory. Alternatively, one may say that the Baxter-Wu model is designed so that the amplitude of the marginally irrelevant operator is set to zero. The Baxter-Wu universality class is also described via its universal amplitude ratios in Ref. [11].

Both models, the Hintermann–Merlini (HM) and the Baxter–Wu (BW) models, had many features in common: they were defined on plane triangulations (i.e., all faces were triangles), the dynamical variables were Ising spins, and the Hamiltonian only included 3-spin terms (one for each triangular face). These two models belong to a more general family of models, that we will denote as the Hintermann–Merlini–Baxter–Wu (HMBW) model. We define this model on any plane triangulation $G = (V, E)$ of vertex set V and edge set E . Then on each vertex $x \in V$ we place an Ising spin $\sigma_x = \pm 1$. These spins interact through the Hamiltonian:¹

$$\mathcal{H}_{\text{HMBW}} = -J \sum_{\triangle=\{i,j,k\}} \sigma_i \sigma_j \sigma_k, \quad (1.1)$$

where the sum is over all triangular faces $\triangle = \{i, j, k\}$ of G , and J is a coupling

¹ We could define the HMBW model with face-dependent couplings; but we will not need this generalization in this paper. This comment also applies to the other models considered here.

constant. This kind of models (and generalizations of them) were already considered by other authors [12, 13] from a group-theoretical point of view. In this paper, we will focus on the particular case of Eulerian triangulations: a graph is Eulerian if the degree of all its vertices is even. This property will play an important role in the following sections.

The second research line produced (among others) the so-called Ashkin–Teller (AT) model [14]. This model was introduced in 1943 and generalized the Ising model to a 4-state model. It was soon recognized that it could be written as two coupled Ising models [15]. More precisely, given a graph $G = (V, E)$, we place on each vertex $x \in V$ of the graph *two* spins σ_i, τ_i . These spins interact via the Hamiltonian:

$$\mathcal{H}_{\text{AT}} = - \sum_{e=\langle ij \rangle \in E} [K_2 \sigma_i \sigma_j + K'_2 \tau_i \tau_j + K_4 \sigma_i \sigma_j \tau_i \tau_j] , \quad (1.2)$$

where the sum is over all edges of the graph. We are not aware of any exact solution to this model, or to any of its particular symmetric case, to be reviewed in Section 3). This AT model contains, as particular cases, the Ising and the 4-state Potts models.

Furthermore, in the symmetric case $K'_2 = K_2$, there is a curve in the (K_2, K_4) -plane that can be mapped to a soluble 6-vertex model [3]. This curve is self-dual, and part of it is critical, with critical exponents varying continuously as we move along that curve. This phenomenon provides the simplest counter-example to the usual notion of universality.

At first sight, the relation between the HMBW and the AT models is rather weak: both models can be defined in terms of Ising spins, and we can find the 8-vertex model in both the solution of the HM model, and in the computation of the self-dual curve of the symmetric AT model. One of the goals of this paper is to show that the relation is deeper: there is an exact mapping between the HMBW model and an infinite-coupling-limit of the AT model (ICLAT), to be defined below. In particular, certain curves in the phase diagram of the ICLAT model on a graph G are equivalent via those mappings to a HMBW model on a certain triangulation G' .

In order to achieve our main goal, we need to work out a series of exact mappings among the HMBW, ICLAT, AT models and some other models we will introduce in Section 3. Some of them are already known results in the literature, others are alternative versions of known results, and finally, some of them are new.

As an application, our last goal is to compute the phase diagram of the ICLAT model on the square, triangular, hexagonal, and kagome lattices, which include one or two HMBW models as particular cases. In all cases, we find a point which corresponds to the point where the self-dual curve of the AT model on the corresponding lattice hits the ICLAT plane. This point is denoted B in Section 5. For the first three lattices, point B belongs to a subspace of the ICLAT model that can be mapped onto the HMBW model. So we can approach it following two independent paths: either along the HMBW subspace, or by considering the limit of large couplings of the self-dual curve of the corresponding AT model. For these lattices we can make predictions of the critical exponents along these two paths, and it turns out that they differ.

The paper is organized as follows. In Section 2 we will show the graph-theoretic set-up. In Section 3 we will define carefully the distinct models we will consider in this paper. In Section 4 we will work out the mappings between the AT and mixed AT models, the mapping between the mixed AT and the ICLAT models, and finally the partial trace transformation. This latter mapping allows us to relate the HMBW and the ICLAT models on certain lattices. We conclude this section with a nice mapping between the BW model and a loop model. The next Section 5 is devoted to the description of the ICLAT phase diagrams for several common lattices: square, triangular, hexagonal, and kagome. In addition we provide the critical exponents for the limiting point of the AT self-dual curve when the couplings tend to infinity. Finally, in Section 6 we summarize our findings. In Appendix A we describe the decimation transformation and how it is related to the partial-trace transformation.

2 Graph-theoretic preliminaries

In this section we will introduce the main lattices where we will define our physical models of Section 3.

Let us consider a graph $G = (V, E)$ with vertex set V , edge set E , and embedded in the plane (i.e, G is planar). We can always define the *dual graph* $G^* = (V^*, E^*)$ of G in the standard way as follows: To each face f in G , there corresponds a dual vertex $f^* \in V^*$; and for every edge $e \in E$, we draw a dual edge $e^* \in E^*$. If the original edge e lies on the intersection of two faces f and h (possibly $f = h$), then the corresponding dual edge e^* joins the dual vertices $f^*, h^* \in V^*$. We can draw G and G^* in the plane in such a way that each edge $e \in E$ intersects its corresponding dual edge $e^* \in E^*$ exactly once.

A graph G is a *plane triangulation* if it is planar and if every face of G (including the outer one) is bounded by a triangle. If G is a plane triangulation, then G^* is a planar cubic graph (i.e., a planar 3-regular graph). Therefore, if G is an Eulerian plane triangulation (i.e., all vertices have even degree), then G^* is a bipartite cubic graph. This implies the following theorem due to Heawood [16, Exercise 18, Chapter 6] (see also [17]):

Theorem 2.1 *A plane triangulation is 3-colorable if and only if it is Eulerian.*

Remarks. 1. In the above theorem, 3-colorable means that we can color the vertices of G with three colors in such a way that two adjacent vertices are not colored alike.

2. This theorem holds for arbitrary Eulerian plane triangulations. In particular, we allow for multiple edges. Let us show a simple example. For any $k \geq 2$, the graph G_k consists of a pair of vertices connected by $2k$ paths, alternating (as one draws the graph on a plane) of lengths 1 and 2. The smallest example G_2 is depicted in Figure 1.

3. Given a Eulerian plane triangulation, then it is *uniquely* 3-colorable (modulo global color permutations).

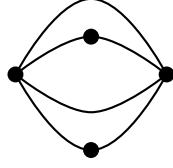


Figure 1: Graph G_2 which is an Eulerian plane triangulation.

As a result, given any Eulerian plane triangulation, there is a *unique* way to split the vertex set into three subsets $V = V_1 \cup V_2 \cup V_3$, such that they are mutually disjoint (i.e., $V_i \cap V_j = \emptyset$ for all $j \neq i$), and for each edge $e \in E$, its endpoints belong to different subsets (i.e., if $e = \{a, b\} \in E$, then $a \in V_i$ and $b \in V_j$ for $i \neq j$). Furthermore, the edge set can also be partitioned into three disjoint sets $E = E_{12} \cup E_{13} \cup E_{23}$, such that any edge $e = \{a, b\} \in E_{ij}$ has one of its endpoints in V_i and the other one in V_j with $i \neq j$.

The dual $G^* = (V^*, E^*)$ of an Eulerian plane triangulation $G = (V, E)$ is a bipartite cubic graph. Therefore, we can properly color the vertices of the dual graph G^* with two colors, or equivalently, we can color the faces of G with two colors in such a way that any two neighboring faces (i.e., two faces with a common edge) are not colored alike. Therefore, this proper face 2-coloring induces a partition of the (triangular) faces $F = F(G)$ into two disjoint sets $F = F_1 \cup F_2$, such that all faces in F_i are colored i . For a plane triangulation G , the following identity follows from the handshake lemma on G^* : $|E| = 3|F|/2$, which implies using Euler's formula $|E| - |V| = |F| - 2$, that the number of faces $|F|$ is even: $|F| = 2(|V| - 2)$. Furthermore, $|F_1| = |F_2| = |V| - 2$, because G^* is 3-regular.

A graph G is a *plane quasi-triangulation* if it is planar and if every face of G (except the outer one) is bounded by a triangle. This outer face is bounded by a cycle of length $\ell \geq 4$. Plane quasi-triangulation are useful when considering a finite piece of a regular lattice with free boundary conditions: see e.g., Figure 2. If G is a plane quasi-triangulation with an outer face bounded by a cycle of length $\ell \geq 4$, we have to make some modifications to the above results. On one side, if the degree of all inner vertices is even, then the quasi-triangulation is 3-colorable. On the other hand, if there are no bridges it is also uniquely 3-colorable (modulo global color permutations).

The number of faces is $|F| = |F_{\text{in}}| + 1$, where $|F_{\text{in}}|$ is the number of inner triangular faces. Then the number of edges is given by $|E| = (3|F_{\text{in}}| + \ell)/2$. Therefore, $|F_{\text{in}}|$ and ℓ should have the same parity, as $|E|$ is an integer. The number of triangular faces is given by $|F_{\text{in}}| = 2|V| - \ell - 2$. Therefore, we need an outer cycle of even length to have an even number of inner triangular faces.

The dual of a plane quasi-triangulation with all the inner vertices of even degree is a graph $G^* = (V^*, E^*)$ constructed as follows: the vertex set $V^* = V_{\text{in}}^* \cup \{v_{\text{out}}^*\}$ contains a vertex $v^* \in V_{\text{in}}^*$ for each inner triangular face in G , and an additional vertex v_{out}^* accounting for the outer face in G . The former vertices have degree three, and the latter has degree ℓ . The edge set E^* is constructed in the usual way. The

subgraph induced by the inner vertices V_{in}^* is indeed bipartite, so the set of inner faces F_{in} can also be split into two disjoint sets $F_{\text{in}} = F_1 \cup F_2$. However, we cannot ensure that both sets F_i have the same cardinality, as the dual graph G^* is not regular.

We are going to study two classes of plane triangulations: the standard triangular lattice (which is a 6-regular graph), and the infinite family of Eulerian plane triangulations introduced in [18].

2.1 Triangular lattice

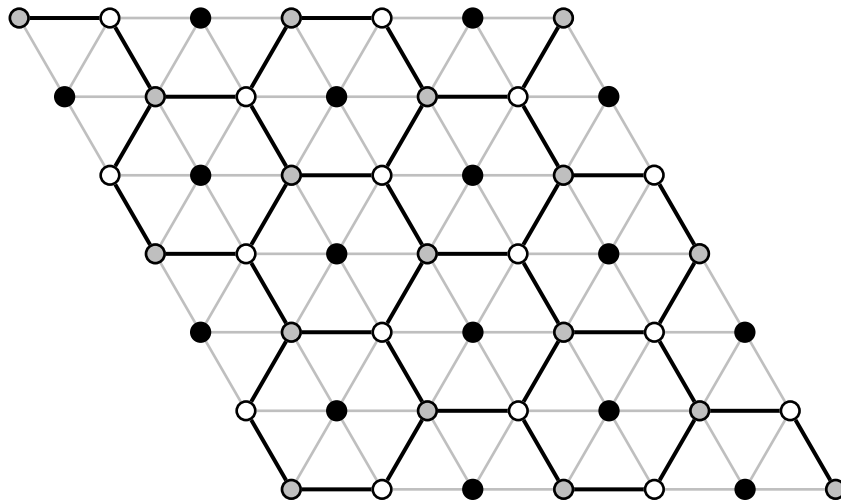


Figure 2: Triangular lattice of size 7×7 with free boundary conditions. The vertex set has a partition into three disjoint sets, depicted as gray, white, and black dots. The edge set is formed by the black and gray edges. The black edges show the subgraph $G_{12} = (V_1 \cup V_2, E_{12})$, which is a hexagonal lattice.

An infinite triangular lattice $G = (V, E)$ is a 6-regular triangulation of the infinite plane, as shown in Figure 2. It is uniquely 3-colorable, therefore we can split the vertex set into three disjoint subsets: $V = V_1 \cup V_2 \cup V_3$. Note that for each $i \neq j$, the subgraph $G_{ij} = (V_i \cup V_j, E_{ij})$ forms a hexagonal lattice.

The dual lattice $G_{ij}^* = (V_k, E^*)$ contains as a vertex set the third subset V_k ($k \neq i, j$) of V . This also works on the other way around: for each $i = 1, 2, 3$, the vertex set V_i can be regarded as the vertex set of another triangular lattice (with larger lattice spacing), and whose dual is precisely the hexagonal lattice $G_{jk} = (V_j \cup V_k, E_{jk})$ with $i \neq j, k$. For instance, in Figure 2 the white and gray dots and all the black edges form a hexagonal lattice, whose dual has a vertex set formed by the black dots.

A finite piece of the triangular lattice is a finite subset of the infinite lattice described above with linear dimensions $L_x \times L_y$ and free boundary conditions. Figure 2 shows an example with $L_x = L_y = 7$. This is a plane quasi-triangulation; but it is not Eulerian, as there are precisely two vertices with odd degree (the top right and

the bottom left corners). All the inner vertices i have degree $d_i = 6$, but the degree of the vertices belonging to the outer cycle can be 2, 3, or 4. The length of this outer cycle is $\ell = 2(L_x + L_y - 2)$. In order to obtain an Eulerian plane triangulation from this graph, we proceed as follows:

- (a) Add an edge f joining the two vertices with odd degree. We obtain an Eulerian graph with all faces being triangles, except two, which are bounded by cycles of length $\ell' = L_x + L_y - 1$.
- (b) If ℓ' is not a multiple of 3, then subdivide the extra edge with 1 (resp. 2) vertices when $\ell' \equiv 2 \pmod{3}$ (resp. $\ell' \equiv 1 \pmod{3}$). So we end with two faces bounded by cycles of length multiple of 3, and all vertices along this cycle have even degree.
- (c) Take one cycle, and number the vertices 1, 2, 3 according to the sublattice V_i the vertex belongs to. Then form triangular faces by adding one edge between two vertices labeled 1 and 3, with a single vertex labeled 2 in between.
- (d) We obtain one cycle of even length with all vertices of odd degree (as in the previous step we added a single edge to each vertex). The vertices on this cycle are labeled alternatively 1 and 3. Now place a new vertex (labeled 2) inside the face bounded by this cycle. Then add edges between this new vertex and any of the vertices defining the cycle. Indeed, the degree of all vertices is now even.
- (e) Repeat the last two steps on the other cycle of length multiple of 3.

In this way, from a finite subset of linear size $L_x \times L_y$ of a triangular lattice with free boundary conditions, we have produced an Eulerian plane triangulation. Indeed, the added vertices and edges are a negligible fraction of the total number of vertices and edges, when $L_x, L_y \rightarrow \infty$. Therefore, we expect that their contribution to the infinite-volume free energy would be zero.

2.2 A family of Eulerian plane triangulations

In this section, we follow Ref. [18]. Let us construct this family of Eulerian planar triangulation by starting from a connected planar graph $G = (V, E)$. We can then define its dual $G^* = (V^*, E^*)$. The next step is to build the graph $\widehat{G} = (V \cup V^*, \widehat{E})$ with vertex set $V \cup V^*$ and edges ij whenever $i \in V$ lies on the boundary of the face of G that contains $j \in V^*$. The graph \widehat{G} is a plane quadrangulation: on each face of \widehat{G} , one pair of diametrically opposite vertices corresponds to an edge $e \in E$, and the other pair corresponds to an edge $e^* \in E^*$. In other words, \widehat{G} is the dual of the medial graph $\mathcal{M}(G) = \mathcal{M}(G^*)$. Conversely, every quadrangulation \widehat{G} arises via this construction from some pair G, G^* . (See [18, Figure 1].) The vertices of G (resp. G^*) are depicted gray (resp. white), and the edges in \widehat{E} are depicted as solid black lines in Figure 3.

Let us now define the graph \widetilde{G} constructed from \widehat{G} by adjoining a new vertex in each face of \widehat{G} , and four new edges connecting this new vertex to the four corners of the

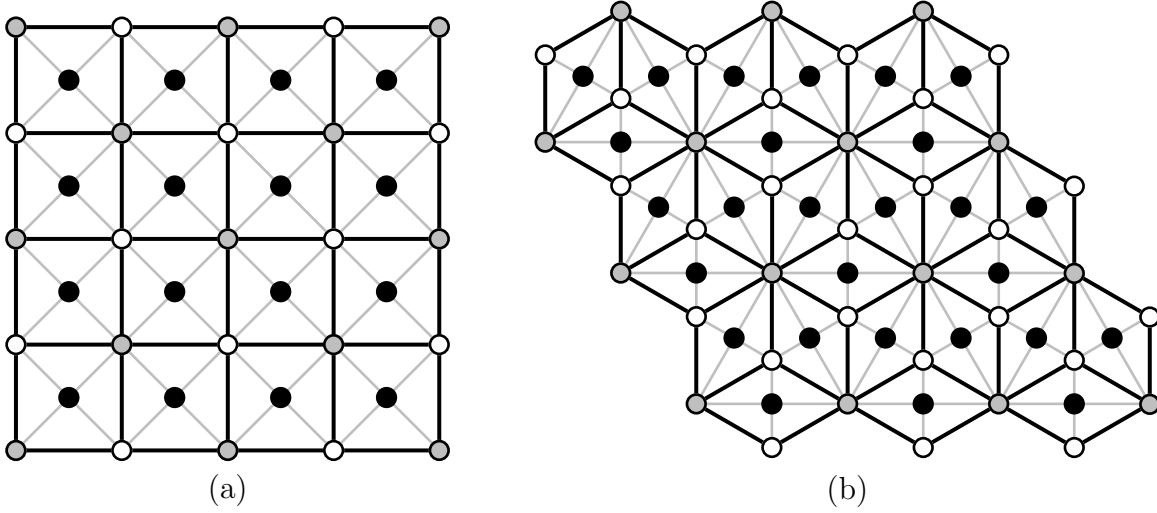


Figure 3: Two pieces of planar triangulations with free boundary conditions: (a) the union-jack lattice of size 5×5 , and (b) the bisected hexagonal lattice of size 4×4 (measured in units of the underlying triangular Bravais lattice i.e., the gray dots). The vertex set has a partition into three disjoint sets, depicted as gray, white, and black dots. The gray and white dots and the black solid lines form the lattice \hat{G} : square (a) and diced (b). The new vertices and edges added to \hat{G} to get \tilde{G} are depicted as black dots and solid gray lines, respectively.

face. The new vertex is depicted as a black dot, and the new edges as solid gray lines in Figure 3. The graph \tilde{G} is an Eulerian plane triangulation, with vertex tripartition $V = V \cup V^* \cup V_3$, where V_3 is the set consisting of the new degree-4 vertices. Conversely, every Eulerian plane triangulation in which one sublattice consists of degree-4 vertices arises in this way. Indeed, this does not cover the triangular lattice.

If $G = G^* = \hat{G} = \text{square lattice}$, then $\tilde{G} = \text{union-jack lattice}$, displayed in Figure 3(a). If $G = \text{triangular lattice}$, $G^* = \text{hexagonal lattice}$, then $\hat{G} = \text{diced lattice}$, and $\tilde{G} = \text{bisected hexagonal lattice}$, displayed in Figure 3(b). According to the standard notation [19], the union-jack lattice is the $[4 \cdot 8^2]$ Leaves tiling, and the bisected hexagonal lattice corresponds to the Leaves tiling $[4 \cdot 6 \cdot 12]$.

The infinite union-jack lattice is not regular since $d_i = 8$ for all $i \in V \cup V^*$, while $d_i = 4$ for all $i \in V_3$. This lattice can be regarded as a square Bravais lattice with a two-point basis. Notice that the union-jack lattice satisfies the following properties:

- The graph $\hat{G} = (V \cup V^*, \hat{E})$ has a square-lattice dual $\hat{G}^* = (V_3, \hat{E}^*)$.
- The subgraph $G_{13} = (V \cup V_3, E_{13})$, where E_{13} are the set of edges joining vertices $e = \{ij\}$ with $i \in V$ and $j \in V_3$, can be regarded as a decorated square lattice tilted 45° with respect the original lattice. Its dual is another tilted square lattice $G_{13}^* = (V^*, E_{13}^*)$, where every edge in G_{13}^* is doubled. The same occurs to the subgraph $G_{23} = (V^* \cup V_3, E_{23})$.

The bisected hexagonal lattice is also non-regular: the degrees of the vertices in V (gray dots), V^* (white dots), and V_3 (black dots) are respectively 12, 6, and 4 (see Figure 3(b)). This lattice can be regarded as a triangular Bravais lattice (formed by the vertices in V) with a 6-point basis. Notice that the bisected hexagonal lattice satisfies the following properties:

- The graph $\widehat{G} = (V \cup V^*, \widehat{E})$ is a diced lattice, and its dual is $\widehat{G}^* = (V_3, \widehat{E}^*)$ which is a kagome lattice.
- The subgraph $G_{13} = (V \cup V_3, E_{13})$, where E_{13} are the set of edges joining vertices $e = \{ij\}$ with $i \in V$ and $j \in V_3$, can be regarded as a decorated triangular lattice. Its dual is the hexagonal lattice $G_{13}^* = (V^*, E_{13}^*)$, where every edge in G_{13}^* is doubled.
- The subgraph $G_{23} = (V^* \cup V_3, E_{23})$, where E_{23} are the set of edges joining vertices $e = \{ij\}$ with $i \in V^*$ and $j \in V_3$, can be regarded as a decorated hexagonal lattice. Its dual is the triangular lattice $G_{23}^* = (V, E_{23}^*)$, where every edge in G_{23}^* is doubled.

The union-jack and bisected-hexagonal lattices with free boundary conditions shown in Figure 3 are quasi triangulations. But in both cases it is very easy to modify them slightly so they become Eulerian triangulations: it suffices to add an outer vertex belonging to V_3 (black dot) and join this extra vertex to every vertex on the outer cycle of each graph. As the degree of all of them was odd, with the new edge, it becomes even, and we obtain the desired Eulerian plane triangulation.

3 Models to be studied

In this section we will introduce the models we are going to use in the following sections, and study their main properties. We cover a well-known model (the AT model [14]), a model known in the literature in a different context (the HMBW model [2, 12, 13]), a model used as a mere technical step (but we think it has some interest in its own right: the mixed AT model [3]), and a *new* model (the infinite-coupling limit AT model).

3.1 HMBW model on an Eulerian plane triangulation

Given an Eulerian plane triangulation $G = (V, E)$ with vertex set V , edge set E , and the set $F(G)$ of all the *triangular* faces, we define the *Hintermann–Merlini–Baxter–Wu model* (HMBW) on G as follows: on each vertex $i \in V$, we place an Ising spin $\sigma_i = \pm 1$, and these spins interact via the Hamiltonian:

$$\mathcal{H}_{\text{HMBW}} = -J \sum_{\{i,j,k\}=t \in F(G)} \sigma_i \sigma_j \sigma_k, \quad (3.1)$$

where the sum is over all the triangular faces $t = \{i, j, k\}$ of G bounded by the vertices i, j, k , and the corresponding 3-spin interaction has a coupling constant J . The partition function is

$$Z_{\text{HMBW}}(G; J) = \sum_{\{\sigma\}} e^{-\mathcal{H}_{\text{HMBW}}} . \quad (3.2)$$

In the ferromagnetic regime $J \geq 0$, if G is a plane Eulerian triangulation the HMBW model has exactly four ground states: one in which all spins take the same value $\sigma = +1$, and three states in which one spin takes the value $\sigma = +1$, and the other two take the opposite value.

One important property of the ferromagnetic HMBW model on an Eulerian plane triangulation is that this model is self-dual [13] with dual coupling satisfying the identity

$$v v^* = 2 , \quad (3.3)$$

where the temperature-like variable v is defined as

$$v = e^{2J} - 1 . \quad (3.4)$$

This self-dual point satisfies:

$$v_c = \sqrt{2} \quad (3.5a)$$

$$e^{2J_c} = 1 + \sqrt{2} \quad (3.5b)$$

In the BW and HM models this self-dual point (3.5) constitutes the *unique* critical point of the model, as the exact solution shows [2, 4, 5]. Notice that the critical coupling (3.5b) is the same as the critical coupling for the square-lattice Ising model [1].

3.2 The Ashkin–Teller model

Let us consider an arbitrary graph $G = (V, E)$, with vertex set V and edge set E . The *Ashkin–Teller model* (AT) is defined on G as follows: on each vertex $i \in V$ we place two Ising spins $\sigma_i, \tau_i = \pm 1$, and these spins interact via the Hamiltonian (1.2) [14]. Therefore, we can regard this system as two copies of the graph G , with the σ spins living on one copy, and the τ spins living on the other. The σ (resp. τ) spins interact among themselves via a nearest-neighbor coupling K_2 (resp. K'_2), and both copies interact via a 4-spin coupling K_4 . The partition function for this system is

$$Z_{\text{AT}}(G; K_2, K'_2, K_4) = \sum_{\{\sigma, \tau\}} e^{-\mathcal{H}_{\text{AT}}} . \quad (3.6)$$

The Boltzmann weight for each edge $e = \langle ij \rangle$ can be read from (1.2)/(3.6), and depends only on the products $\sigma_i \sigma_j, \tau_i \tau_j = \pm 1$:

$$\omega_{ij}(\sigma_i \sigma_j, \tau_i \tau_j) = \exp [K_2 \sigma_i \sigma_j + K'_2 \tau_i \tau_j + K_4 \sigma_i \sigma_j \tau_i \tau_j] . \quad (3.7)$$

Indeed, the weights ω_{ij} are the same for all edges $\langle ij \rangle \in E$. For each edge $\langle ij \rangle \in E$, there are four possible spin configurations. Their corresponding weights are denoted by ω_k with $k = 0, 1, 2, 3$, and they are given in the second column of Table 1. We use the standard definitions (see e.g., Ref. [20]):

$$\omega_0 = \omega_{ij}(+1, +1) \quad (3.8a)$$

$$\omega_1 = \omega_{ij}(+1, -1) \quad (3.8b)$$

$$\omega_2 = \omega_{ij}(-1, +1) \quad (3.8c)$$

$$\omega_3 = \omega_{ij}(-1, -1) \quad (3.8d)$$

We can also use these weights (3.8) to define the corresponding AT model:

$$Z_{\text{AT}}(G; K_2, K'_2, K_4) \equiv Z_{\text{AT}}(G; \omega_0, \omega_1, \omega_2, \omega_3). \quad (3.9)$$

The values of the couplings K_2, K'_2, K_4 in terms of the weights $\omega_0, \omega_1, \omega_2, \omega_3$ can be obtained from the equations given in the second column of Table 1:

$$e^{4K_0} = \omega_0 \omega_1 \omega_2 \omega_3 \quad (3.10a)$$

$$e^{4K_2} = \frac{\omega_0 \omega_1}{\omega_2 \omega_3} \quad (3.10b)$$

$$e^{4K'_2} = \frac{\omega_0 \omega_2}{\omega_1 \omega_3} \quad (3.10c)$$

$$e^{4K_4} = \frac{\omega_0 \omega_3}{\omega_1 \omega_2} \quad (3.10d)$$

where K_0 is an arbitrary constant fixing the zero of energy. In Eq. (1.2) we choose $K_0 = 0$ for simplicity; therefore the weights ω_k satisfy:

$$\omega_0 \omega_1 \omega_2 \omega_3 = 1. \quad (3.11)$$

For our purposes, it is also interesting to compute the normalized weights obtained by making the weight corresponding to the configuration $\sigma_i = \sigma_j, \tau_i = \tau_j$ equal to one (i.e., $\omega_0 = 1$). These normalized weights are also displayed in the third column of Table 1.

The AT model (1.2)/(3.6) contains two important particular cases: when $K_4 = 0$, we obtain two decoupled Ising models with couplings K_2 and K'_2 . At the other extreme, the limit $K_4 \rightarrow +\infty$ corresponds to a single Ising model ($\sigma = \tau$) with coupling $K_2 + K'_2$. Finally, the line $K_2 = K'_2 = K_4$, corresponds to the 4-state Potts model with $J_{\text{Potts}} = 4K_2$.

The Hamiltonian (1.2) is invariant under any permutation π of the coupling constants (K_2, K'_2, K_4) , as the fields $\sigma, \tau, \sigma\tau$ play symmetric roles in the model:

$$(K_2, K'_2, K_4) \rightarrow \pi(K_2, K'_2, K_4), \quad \pi \in S_3. \quad (3.12)$$

If the graph G is *bipartite*, then the vertex set can be split into two disjoint sets $V = V_1 \cup V_2$, such that each edge $e = \langle ij \rangle$ satisfies that $i \in V_i$ and $j \in V_j$ with $i \neq j$.

Configuration	Weight	(Normalized) Weight
$\sigma_i \sigma_j = +1, \tau_i \tau_j = +1$	$\omega_0 = e^{K_0 + K_2 + K'_2 + K_4}$	1
$\sigma_i \sigma_j = +1, \tau_i \tau_j = -1$	$\omega_1 = e^{K_0 + K_2 - K'_2 - K_4}$	$e^{-2(K'_2 + K_4)}$
$\sigma_i \sigma_j = -1, \tau_i \tau_j = +1$	$\omega_2 = e^{K_0 - K_2 + K'_2 - K_4}$	$e^{-2(K_2 + K_4)}$
$\sigma_i \sigma_j = -1, \tau_i \tau_j = -1$	$\omega_3 = e^{K_0 - K_2 - K'_2 + K_4}$	$e^{-2(K_2 + K'_2)}$

Table 1: Boltzmann weights for the AT model (1.2)/(3.6). For each edge $\langle ij \rangle \in E$, we first give the configuration of the corresponding σ, τ variables, we then quote the weight read off from (3.7) [“Weight”], and the normalized weight obtained by making the first one equal to 1 [“(Normalized) Weight”]. K_0 is an arbitrary constant fixing the zero of energy for the contribution of each edge $\langle ij \rangle \in E$. In (1.2) we choose $K_0 = 0$ for simplicity.

In this case, there are additional symmetries because we can flip σ , τ , or both, on any of two vertex subsets V_i . Then, the uniform AT model on a bipartite graph G is invariant under the transformations:

$$(K_2, K'_2, K_4) \rightarrow (-K_2, K'_2, -K_4) \quad (3.13a)$$

$$(K_2, K'_2, K_4) \rightarrow (K_2, -K'_2, -K_4) \quad (3.13b)$$

$$(K_2, K'_2, K_4) \rightarrow (-K_2, -K'_2, K_4) \quad (3.13c)$$

When $K_2 = K'_2$ we obtain the *symmetric Ashkin–Teller model*:

$$\mathcal{H}_{\text{sAT}} = - \sum_{\langle ij \rangle \in E} [K_2(\sigma_i \sigma_j + \tau_i \tau_j) + K_4 \sigma_i \sigma_j \tau_i \tau_j] . \quad (3.14)$$

3.3 The Infinite-Coupling Limit Ashkin–Teller model

As far as we can tell this model is new in the literature.² Its motivation is rather simple: if we look at the normalized weights in Table 1, we see that in the limit $K_2, K'_2, -K_4 \rightarrow +\infty$, with $K_2 + K_4 = L_2$ and $K'_2 + K_4 = L'_2$ kept finite, one has that the normalized weight for $\sigma_i \sigma_j = \tau_i \tau_j = -1$ tends to zero, while the other configurations keep nonzero normalized weights. These weights correspond to the *infinite-coupling-limit Ashkin–Teller model* (ICLAT). The Hamiltonian of this model can be alternatively written as:

$$\mathcal{H}_{\text{ICLAT}} = - \sum_{\langle ij \rangle \in E} [(L_2 - L)\sigma_i \sigma_j + (L'_2 - L)\tau_i \tau_j + L\sigma_i \sigma_j \tau_i \tau_j] , \quad (3.15)$$

² After the completion of this work, we learned that a particular case of this model had been previously considered by Ikhlef and Rajabpour [21]. Their findings have been summarized in a remark in Section 5.1. We thank the referee for bringing this paper to our attention.

where we take the limit $L \rightarrow -\infty$, with the couplings L_2, L'_2 kept finite. The corresponding partition function is

$$Z_{\text{ICLAT}}(G; L_2, L'_2) = \lim_{L \rightarrow -\infty} \sum_{\{\sigma, \tau\}} e^{-\mathcal{H}_{\text{ICLAT}}} . \quad (3.16)$$

The Boltzmann weight for a given edge $e = \langle ij \rangle$ is given by (3.15)/(3.16) and it reads:

$$\omega(\sigma_i \sigma_j, \tau_i \tau_j) = \exp[(L_2 - L) \sigma_i \sigma_j + (L'_2 - L) \tau_i \tau_j + L \sigma_i \sigma_j \tau_i \tau_j] . \quad (3.17)$$

The values of this weight for the four possible spin configuration are given in Table 2. Indeed, if we normalize these weights so that the normalized weight for $\sigma_i \sigma_j = \tau_i \tau_j = 1$ is equal to one (see the third column in Table 2), we obtain the same weights as those obtained by taking the appropriate infinite-coupling limit in the normalized weights for the AT model (displayed in the third column in Table 1).

Configuration	Weight	(Normalized) Weight
$\sigma_i \sigma_j = +1, \tau_i \tau_j = +1$	$\omega_0 = e^{L_0 + L_2 + L'_2 - L}$	1
$\sigma_i \sigma_j = +1, \tau_i \tau_j = -1$	$\omega_1 = e^{L_0 + L_2 - L'_2 - L}$	$e^{-2L'_2}$
$\sigma_i \sigma_j = -1, \tau_i \tau_j = +1$	$\omega_2 = e^{L_0 - L_2 + L'_2 - L}$	e^{-2L_2}
$\sigma_i \sigma_j = -1, \tau_i \tau_j = -1$	$\omega_3 = e^{L_0 + 3L - L_2 - L'_2}$	$e^{2(2L - L_2 - L'_2)} \rightarrow 0$

Table 2: Boltzmann weights for the ICLAT model (3.15)/(3.16). For each edge $\langle ij \rangle \in E$, we first give the configuration of the corresponding σ, τ variables, we then quote the weight read off from (3.17) [“Weight”], and the normalized weight obtained by making the first one equal to 1 [“(Normalized) Weight”] in the limit $L \rightarrow -\infty$. L_0 is an arbitrary constant fixing the zero of energy for the contribution of each edge $\langle ij \rangle \in E$. In (3.15) we choose $L_0 = 0$ for simplicity.

When $L_2 \rightarrow +\infty$, then the σ spins are all equal; therefore, the model reduces to an Ising model on the τ spins with coupling L'_2 . Indeed, when $L'_2 \rightarrow +\infty$, the τ spins are all equal, and the model reduces to an Ising model on the σ spins with coupling L_2 .

In the ICLAT model (3.15) σ and τ play a symmetric role, therefore, the model is invariant under the transformation

$$(L_2, L'_2) \rightarrow (L'_2, L_2) . \quad (3.18)$$

If the graph G is *bipartite*, we can define a new spin $\rho_i = \sigma_i \tau_i = \pm 1$, so that the Hamiltonian (3.15) reads:

$$\mathcal{H}_{\text{ICLAT}} = - \sum_{\langle ij \rangle \in E} [(L_2 - L) \sigma_i \sigma_j + (L'_2 - L) \rho_i \rho_j \sigma_i \sigma_j + L \rho_i \rho_j] , \quad (3.19)$$

when $L \rightarrow -\infty$. If we flip the spins ρ_i on one of two vertex subsets V_i , then the model is invariant under the transformation $(L_2 - L, L'_2 - L, L) \rightarrow (L_2 - L, L - L'_2, -L)$. We obtain

$$\mathcal{H}_{\text{ICLAT}} = - \sum_{\langle ij \rangle \in E} [(L_2 - L)\sigma_i\sigma_j - (L'_2 - L)\rho_i\rho_j\sigma_i\sigma_j - L\rho_i\rho_j], \quad (3.20)$$

in the limit $L \rightarrow -\infty$. By comparing (3.15)/(3.20), we see that, if we redefine $L \rightarrow L + L'_2 \rightarrow -\infty$, we obtain the equivalent Hamiltonian

$$\mathcal{H}_{\text{ICLAT}} = - \sum_{\langle ij \rangle \in E} [(L_2 - L'_2 - L)\sigma_i\sigma_j + (-L'_2 - L)\rho_i\rho_j + L\rho_i\rho_j\sigma_i\sigma_j], \quad (3.21)$$

in the limit $L \rightarrow -\infty$. Therefore, the ICLAT model on a bipartite graph is invariant under the transformations:

$$(L_2, L'_2) \rightarrow (L_2 - L'_2, -L'_2) \quad (3.22a)$$

$$(L_2, L'_2) \rightarrow (-L_2, L'_2 - L_2) \quad (3.22b)$$

where the second equation comes from using the variables (τ, ρ) instead of (σ, ρ) .

If we take $L_2 = L'_2 = 0$ in (3.15), then it reduces to

$$\mathcal{H}_{\text{ICLAT}} = - \sum_{\langle ij \rangle \in E} [-L\sigma_i\sigma_j - L\tau_i\tau_j + L\sigma_i\sigma_j\tau_i\tau_j], \quad (3.23)$$

in the limit $L \rightarrow -\infty$. If the lattice G is bipartite, then we can flip the τ and σ spins on one of the vertex subsets V_i , so that all the couplings become equal to L . So it corresponds to the zero-temperature limit of the antiferromagnetic 4-state Potts model.

3.4 Mixed Ashkin–Teller model

This model appears in a natural way when one consider the duality transformation of an AT model. Let us now suppose that $G = (V, E)$ is an arbitrary planar graph; hence, it has a planar dual pair $G^* = (V^*, E^*)$. Indeed, one can define an AT model on both G or G^* as in the preceding section. However, we can define a *mixed Ashkin–Teller model* (mAT) with one set of spins living on G , and the other set on G^* , and a clever coupling of both Ising models. This coupling is based on the following fact about dual graphs: the number of edges is the same in both G and its dual G^* , and there is natural bijection between these two edge sets: we can always draw G and G^* in the plane in such a way that each edge $e = \langle ij \rangle \in E$ intersects its corresponding dual edge $e^* = \langle i^*j^* \rangle \in E^*$ exactly once.

The formal definition of the mixed AT model is as follows. We place at each vertex $i \in V$ (resp. at each dual vertex $i^* \in V^*$) of the graph G (resp. of the dual graph G^*) an Ising spin $\sigma_i = \pm 1$ (resp. $\tau_{i^*} = \pm 1$), and these spins interact through a nearest-neighbor coupling K_2 (resp. K'_2). These two Ising models are coupled via

the four-spin interaction $K_4\sigma_i\sigma_j\tau_{i^*}\tau_{j^*}$, where $e^* = \langle i^*j^* \rangle \in E^*$ is the unique dual edge associated to the edge $e = \langle ij \rangle \in E$. Therefore, the Hamiltonian for this model is:

$$\mathcal{H}_{\text{mAT}} = -K_2 \sum_{\langle ij \rangle \in E} \sigma_i \sigma_j - K'_2 \sum_{\langle i^*j^* \rangle \in E^*} \tau_{i^*} \tau_{j^*} - K_4 \sum_{\langle ij \rangle \in E} \sigma_i \sigma_j \tau_{i^*} \tau_{j^*}. \quad (3.24)$$

The partition function for this mixed model is given by:

$$Z_{\text{mAT}}(G, G^*; K_2, K'_2, K_4) = \sum_{\substack{\{\sigma_i\} \\ i \in V}} \sum_{\substack{\{\tau_{i^*}\} \\ i^* \in V^*}} e^{-\mathcal{H}_{\text{mAT}}}. \quad (3.25)$$

It is important to note that the spins living on G couple through the coupling K_2 , while those living on its dual G^* , couple via K'_2 .

The notation in (3.24) can be lightened by noting again that the correspondence $\langle ij \rangle \rightarrow \langle i^*j^* \rangle$ is bijective. Thus, we can loosely use the labels ij (instead of i^*j^*) for the τ spins (but one should remember that in the mixed AT model, the τ spins live on the dual vertices V^* , while the σ spins live on V). We can loosely write the Hamiltonian for this model as in Eq. (1.2).

Finally, we can also represent the partition function of the mixed AT model (3.25) in terms of the weights $\{w_k\}$ with $k = 0, 1, 2, 3$ [cf. (3.8)] as in Eq. (3.9):

$$Z_{\text{mAT}}(G, G^*; K_2, K'_2, K_4) \equiv Z_{\text{mAT}}(G, G^*; \omega_0, \omega_1, \omega_2, \omega_3). \quad (3.26)$$

It is important to recall that, if we interchange $G \leftrightarrow G^*$, then we should interchange the couplings $K_2 \leftrightarrow K'_2$, or equivalently, the weights $\omega_1 \leftrightarrow \omega_2$:

$$Z_{\text{mAT}}(G, G^*; K_2, K'_2, K_4) = Z_{\text{mAT}}(G^*, G; K'_2, K_2, K_4) \quad (3.27a)$$

$$= Z_{\text{mAT}}(G^*, G; \omega_0, \omega_2, \omega_1, \omega_3) \quad (3.27b)$$

Remark. Note that, contrary to the standard AT model, the number of σ spins ($= |V|$) is in general different from the number of τ spins ($= |V^*|$).

If $G = (V, E)$ is an Eulerian plane triangulation, then it is 3-colorable, and there is a natural tripartition of the vertex set $V = V_1 \cup V_2 \cup V_3$, and edge set $E = E_{12} \cup E_{13} \cup E_{23}$. If we consider the subgraph $G_{12} = (V_1 \cup V_2, E_{12})$, then its dual subgraph is given by $G_{12}^* = (V_3, E_{12}^*)$, where the dual edge set E_{12}^* is built in the standard way. Then, for each edge $e \in E_{12}$, there corresponds a dual edge $e^* \in E_{12}^*$ such that it crosses e once. Then the Hamiltonian (3.24) can be (loosely) rewritten as

$$\mathcal{H}_{\text{mAT}} = - \sum_{\langle ij \rangle \in E_{12}} [K_2 \sigma_i \sigma_j + K'_2 \tau_i \tau_j + K_4 \sigma_i \sigma_j \tau_i \tau_j], \quad (3.28)$$

and the corresponding partition function (3.25) as

$$Z_{\text{mAT}}(G_{12}, G_{12}^*; K_2, K'_2, K_4) = \sum_{\substack{\{\sigma_i\} \\ i \in V_1 \cup V_2}} \sum_{\substack{\{\tau_{i^*}\} \\ i^* \in V_3}} e^{-\mathcal{H}_{\text{mAT}}}. \quad (3.29)$$

We can also take the same infinite-coupling limit as in the previous section, namely $K_2, K'_2, -K_4 \rightarrow +\infty$, while $L_2 = K_2 + K_4$ and $L'_2 = K'_2 + K_4$ are kept finite. Using the above-discussed bijection between E and E^* , this model can be written loosely as in Eq. (3.15), but again, keeping in mind that the σ (resp. τ) spins live on V (resp. V^*).

4 Mappings among models

4.1 Mapping between the AT and the mixed AT models

In this section we will consider a general AT model with couplings K_2, K'_2, K_4 on a planar graph $G = (V, E)$, not necessarily Eulerian. We assume that either $K'_2 \geq |K_4|$ or $K_2 \geq |K_4|$. Without loss of generality, let us assume that $K'_2 \geq |K_4|$. The relation between the AT and mixed AT models arises when trying to derive the duality relation for the former model. We will follow the ideas of Ref. [20]; but instead of looking for a relation with the 8-vertex model, we will seek the relation with the mixed AT model (3.24)/(3.25). (See also [3, 22, 23].)

Let us start with an AT model on a graph $G = (V, E)$ [cf. (1.2)/(3.6)]:

$$Z_{\text{AT}}(G; K_2, K'_2, K_4) = \sum_{\{\sigma\}} \prod_{\langle ij \rangle \in E} e^{K_2 \sigma_i \sigma_j} \sum_{\{t\}} \prod_{\langle ij \rangle \in E} e^{\tilde{K}_{2ij} t_i t_j}, \quad (4.1)$$

where we have split the sum over the spin configurations into two terms: one over the σ spins, and the other over the t spins (we use the letter t to denote the second set of Ising spins in this case). The effective *edge-dependent* two-spin coupling between the t spins is given by

$$\tilde{K}_{2ij} = K'_2 + K_4 \sigma_i \sigma_j. \quad (4.2)$$

Notice that the condition $K'_2 \geq |K_4|$ implies that $\tilde{K}_{2ij} \geq 0$ for all edges $\langle ij \rangle \in E$.

We now do a high-temperature expansion using the fact that

$$e^{\tilde{K}_{2ij} t_i t_j} = \cosh(\tilde{K}_{2ij}) \left[1 + t_i t_j \tanh(\tilde{K}_{2ij}) \right]. \quad (4.3)$$

When we expand the product over the edges $e \in E$, we get a sum over spanning subgraphs $E' \subseteq E$, where E' is the subset of edges contributing with the factor $t_i t_j \tanh(\tilde{K}_{2ij})$. When we sum over all possible configurations of the t spins, only those subgraphs E' with an *even* number of incident occupied edges on every vertex $x \in V$ survive. In summary, the partition sum reads

$$\begin{aligned} Z_{\text{AT}}(G; K_2, K'_2, K_4) &= 2^{|V|} \sum_{\{\sigma\}} \prod_{\langle ij \rangle \in E} \left[e^{K_2 \sigma_i \sigma_j} \cosh(\tilde{K}_{2ij}) \right] \\ &\quad \times \sum_{\substack{E' \subseteq E \\ E' \text{ Eulerian}}} \prod_{\langle ij \rangle \in E'} \tanh(\tilde{K}_{2ij}), \end{aligned} \quad (4.4)$$

where \tilde{K}_{2ij} is given by (4.2).

We now introduce the new Ising variables $\tau_i = \pm 1$ living on the dual vertex set V^* . They are assigned such that for any Eulerian spanning subgraph (V, E') of $G = (V, E)$:

$$e = \langle ij \rangle \in E' \iff \tau_{i^*} \tau_{j^*} = -1, \quad (4.5)$$

where i^*, j^* are the vertices of the dual edge e^* corresponding to the edge e . (See Figure 4.) In words, given an edge $e \in E$, if this edge belongs (resp. does not belong) to the subset $E' \subseteq E$, then the τ variables associated to this edge have different (resp. equal) signs.

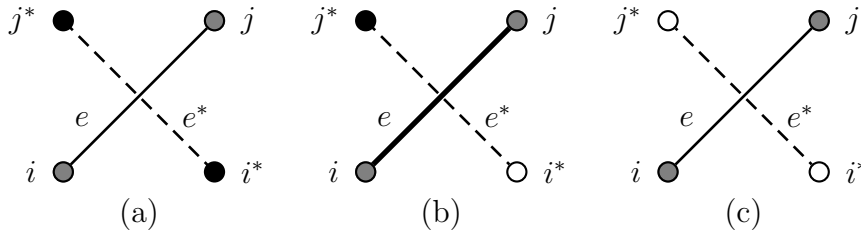


Figure 4: (a) Dual edge $e^* = \langle i^* j^* \rangle \in E^*$ corresponding to an edge $e = \langle ij \rangle \in E$. The vertices i, j belong to V , and the dual ones i^*, j^* to V^* . (b) When e belongs to the spanning subgraph (V, E') (depicted as a thick line), then $\tau_{i^*} \tau_{j^*} = -1$ (depicted as dots of different colors). (c) When e does not belong to the spanning subgraph (V, E') , then $\tau_{i^*} \tau_{j^*} = 1$ (depicted as dots of equal color).

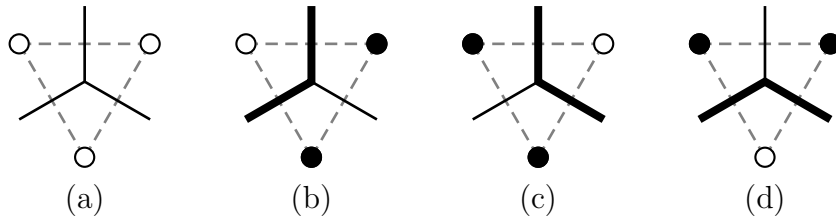


Figure 5: Mapping (4.5) between Eulerian spanning subgraphs on a vertex of degree 3. The solid black (resp. dashed gray) edges belong to E (resp. E^*), and the dots correspond to vertices of V^* . If $e \in E$ belongs (resp. does not belong) to the spanning subgraph (V, E') , the corresponding edge is depicted as a thick (resp. thin) solid black line. In panels (a)–(d) we show the four different configurations: no edge in E' (i.e., all Ising spins have the same value), and two edges in E' (i.e., two Ising spins take the same value, and the other one takes the other value).

For instance, the relation between edge configurations and τ spin configurations for vertices of degree 3 and 4 are given, respectively in Figures 5 and 6. For a vertex

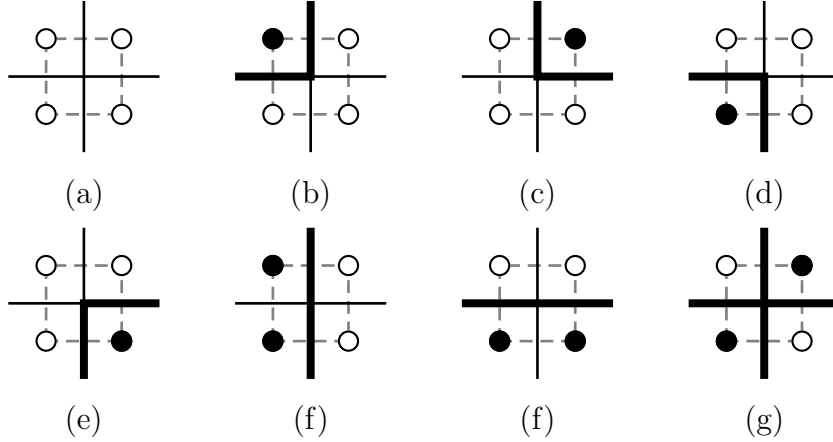


Figure 6: Mapping (4.5) between Eulerian spanning subgraphs i on a vertex of degree 4. In panels (a)–(g) we show the eight different configurations: no edge in E' (i.e., all Ising spins have the same value), two edges in E' (i.e., two consecutive Ising spins take the same value, and the other two take the other value; or one spin takes one value, and the other three spins take the opposite value), and four edges in E' (the spin values alternate as we move around).

$v \in V$ of degree d , the number of possible Eulerian configurations (i.e., an even number of edges incident to v) is given by

$$\sum_{n \geq 0} \binom{d}{2n} = 2^{d-1}, \quad (4.6)$$

which is exactly the same number of τ -spin configurations of the d neighboring vertices (modulo a global reversal of the spin values). Indeed, there is a one-to-two correspondence between edges subsets E' and $\{\tau\}$ configurations: for each subset E' there are two equivalent τ configurations differing by a global change of sign.

Note that the σ (resp. τ) spins live on the vertices of V (resp. V^*). Thus, we arrive at a mixed AT model defined on G and G^* :

$$\begin{aligned} Z_{\text{AT}}(G; K_2, K'_2, K_4) &= 2^{|V|-1} \sum_{\substack{\{\sigma_i\} \\ i \in V}} \sum_{\substack{\{\tau_i\} \\ i \in V^*}} \prod_{\langle ij \rangle \in E} \left[e^{K_2 \sigma_i \sigma_j} \cosh(\tilde{K}_{2ij}) \right] \\ &\quad \times \prod_{\langle ij \rangle \in E} \left[\frac{1 + \tau_i \tau_j^*}{2} + \frac{1 - \tau_i \tau_j^*}{2} \tanh(\tilde{K}_{2ij}) \right] \end{aligned} \quad (4.7a)$$

$$= 2^{|V|-1} \sum_{\substack{\{\sigma_i\} \\ i \in V}} \sum_{\substack{\{\tau_i\} \\ i \in V^*}} \prod_{\langle ij \rangle \in E} \hat{\omega}_{ij}(\sigma_i \sigma_j, \tau_i \tau_j^*) \quad (4.7b)$$

where \tilde{K}_{2ij} is given by (4.2), and to each edge $e = \langle ij \rangle \in E$ there corresponds a unique dual edge $e^* = \langle i^* j^* \rangle \in E^*$, and vice versa. The extra factor 2^{-1} comes

from the above-mentioned two-to-one relation between τ configurations and Eulerian subgraphs $E' \subseteq E$. The second term in the product is just a way to express the fact that when $e \in E'$ (so $\tau_{i*} = -\tau_{j*}$), there is a contribution $\tanh(\tilde{K}_{2ij})$; and when $e \notin E'$, (so $\tau_{i*} = \tau_{j*}$), then the contribution is 1. The Boltzmann weights $\hat{\omega}_{ij}$ associated to the above representation (4.7) are given in Table 3.

Configuration	Weight	(Normalized) Weight
$\sigma_i \sigma_j = +1, \tau_i \tau_j = +1$	$\hat{\omega}_0 = e^{K_2} \cosh(K'_2 + K_4)$	1
$\sigma_i \sigma_j = +1, \tau_i \tau_j = -1$	$\hat{\omega}_1 = e^{K_2} \sinh(K'_2 + K_4)$	$\tanh(K'_2 + K_4)$
$\sigma_i \sigma_j = -1, \tau_i \tau_j = +1$	$\hat{\omega}_2 = e^{-K_2} \cosh(K'_2 - K_4)$	$e^{-2K_{2ij}} \frac{\cosh(K'_2 - K_4)}{\cosh(K'_2 + K_4)}$
$\sigma_i \sigma_j = -1, \tau_i \tau_j = -1$	$\hat{\omega}_3 = e^{-K_2} \sinh(K'_2 - K_4)$	$e^{-2K_2} \frac{\sinh(K'_2 - K_4)}{\cosh(K'_2 + K_4)}$

Table 3: Boltzmann weights for the model (4.7). For each configuration of the σ, τ variables, we first quote the weight (up to an unimportant global factor) read off from (4.7) [“Weight”], and then the normalized weight obtained by making the first one equal to 1 [“(Normalized) Weight”].

The relation between the weights $\hat{\omega}_k$ of the transformed model (4.7) and the original ones ω_k is given for every edge $\langle ij \rangle \in E$ by

$$\hat{\omega}_0 = \frac{1}{2}(\omega_0 + \omega_1) \quad (4.8a)$$

$$\hat{\omega}_1 = \frac{1}{2}(\omega_0 - \omega_1) \quad (4.8b)$$

$$\hat{\omega}_2 = \frac{1}{2}(\omega_2 + \omega_3) \quad (4.8c)$$

$$\hat{\omega}_3 = \frac{1}{2}(\omega_2 - \omega_3) \quad (4.8d)$$

The above results can be summarized in the following

Theorem 4.1 *Let $G = (V, E)$ be a planar graph. Then the Ashkin–Teller model (1.2)/(3.6) on G , with $K'_2 \geq |K_4|$, is equivalent to a mixed Ashkin–Teller model (3.24)/(3.25) on G and G^* such that*

$$Z_{\text{AT}}(G; \omega_0, \omega_1, \omega_2, \omega_3) = 2^{|V|-1} Z_{\text{MAT}}(G, G^*; \hat{\omega}_0, \hat{\omega}_1, \hat{\omega}_2, \hat{\omega}_3), \quad (4.9)$$

where the weights $\hat{\omega}_k$ are given in terms of the weights ω_k by (4.8).

Remark. Let us remind that in the mixed AT model in Theorem 4.1 the σ (resp. τ) spins live on V (resp. V^*). The σ (resp. τ) spins have a nearest-neighbor coupling K_2 (resp. K'_2); and both σ, τ spins interact via a 4-spin coupling K_4 .

The duality transformation for the AT model can be easily obtained from Theorem 4.1 by playing the same game. We want to express the partition function of the original AT model on G in terms of the partition function of another AT model on the dual graph G^* . This is easily done as follows:

$$2^{-|V|+1} Z_{\text{AT}}(G; \omega_0, \omega_1, \omega_2, \omega_3) = Z_{\text{mAT}}(G, G^*; \hat{\omega}_0, \hat{\omega}_1, \hat{\omega}_2, \hat{\omega}_3) \quad (4.10a)$$

$$= Z_{\text{mAT}}(G^*, G; \hat{\omega}_0, \hat{\omega}_2, \hat{\omega}_1, \hat{\omega}_3) \quad (4.10b)$$

$$= 2^{-|V^*|+1} Z_{\text{AT}}(G^*; \omega_0^*, \omega_1^*, \omega_2^*, \omega_3^*) \quad (4.10c)$$

where the first equality is just Theorem 4.1, the second line comes from using the symmetry relation (3.27) for the mixed AT model, and the last one comes from using Theorem 4.1 on the dual graph G^* . The expression of the new weights ω_k^* in terms of the original ones is

$$\omega_0^* = \hat{\omega}_0 + \hat{\omega}_2 = \frac{1}{2}(\omega_0 + \omega_1 + \omega_2 + \omega_3) \quad (4.11a)$$

$$\omega_1^* = \hat{\omega}_0 - \hat{\omega}_2 = \frac{1}{2}(\omega_0 + \omega_1 - \omega_2 - \omega_3) \quad (4.11b)$$

$$\omega_2^* = \hat{\omega}_1 + \hat{\omega}_3 = \frac{1}{2}(\omega_0 + \omega_2 - \omega_1 - \omega_3) \quad (4.11c)$$

$$\omega_3^* = \hat{\omega}_1 - \hat{\omega}_3 = \frac{1}{2}(\omega_0 + \omega_3 - \omega_1 - \omega_2) \quad (4.11d)$$

The above results can be summarized in the following

Theorem 4.2 (Wu [20]) *Let $G = (V, E)$ be a planar graph. Then the Ashkin–Teller model (1.2)/(3.6) on G is equivalent to another Ashkin–Teller model on the dual graph G^* such that*

$$2^{-|V|} Z_{\text{AT}}(G; \omega_0, \omega_1, \omega_2, \omega_3) = 2^{-|V^*|} Z_{\text{AT}}(G^*; \omega_0^*, \omega_1^*, \omega_2^*, \omega_3^*), \quad (4.12)$$

where the weights ω_k^* are given in terms of the weights ω_k by (4.11).

If G is self-dual, then the corresponding AT model is self-dual when the following condition holds:

$$\omega_0 = \omega_1 + \omega_2 + \omega_3. \quad (4.13)$$

This situation occurs for instance for the infinite square lattice.

4.2 Mapping between the mixed AT and the ICLAT models

Let us now explore a little further the relation between the mixed AT on G and G^* , and the AT model on G^* . We know from (4.10)/(4.11) that:

$$Z_{\text{mAT}}(G, G^*; \omega_0, \omega_1, \omega_2, \omega_3) = 2^{-|V^*|+1} Z_{\text{AT}}(G^*; \omega_0^*, \omega_1^*, \omega_2^*, \omega_3^*) \quad (4.14)$$

where the new weights are given by

$$\omega_0^* = \omega_0 + \omega_2 \quad (4.15a)$$

$$\omega_1^* = \omega_0 - \omega_2 \quad (4.15b)$$

$$\omega_2^* = \omega_1 + \omega_3 \quad (4.15c)$$

$$\omega_3^* = \omega_1 - \omega_3 \quad (4.15d)$$

It is easy to see that $\omega_3^* = 0$ if and only if $\omega_1 = \omega_3$. And the last equality holds true if and only if $K_2 = K_4$. In this particular case, we have

$$2^{|V^*|-1} Z_{\text{mAT}}(G, G^*; \omega_0, \omega_1, \omega_2, \omega_1) = Z_{\text{AT}}(G^*; \omega_0^*, \omega_1^*, \omega_2^*, 0) \quad (4.16a)$$

$$= Z_{\text{AT}}\left(G^*; 1, \frac{\omega_1^*}{\omega_0^*}, \frac{\omega_2^*}{\omega_0^*}, 0\right) \prod_{\langle ij \rangle \in E} \omega_0^* \quad (4.16b)$$

But the ratios of these weights are precisely the couplings of the ICLAT model:

$$\frac{\omega_1^*}{\omega_0^*} = e^{-2K_2'^* - 2K_4^*} = e^{-2L_2'^*} \quad (4.17a)$$

$$\frac{\omega_2^*}{\omega_0^*} = e^{-2K_2^* - 2K_4^*} = e^{-2L_2^*} \quad (4.17b)$$

In terms of the original couplings, we get that the couplings of the ICLAT model are given by the expressions:

$$e^{-2L_2'^*} = \frac{\omega_0 - \omega_2}{\omega_0 + \omega_2} = \tanh(2K_2) \quad (4.18a)$$

$$e^{-2L_2^*} = \frac{2\omega_1}{\omega_0 + \omega_2} = \frac{e^{-2K_2'}}{\cosh(2K_2)} \quad (4.18b)$$

The above considerations prove the following

Theorem 4.3 *Let $G = (V, E)$ be a planar graph. Then the mixed Ashkin–Teller model (3.24)/(3.25) on G and G^* with equal couplings $K_2 = K_4$, is equivalent to the infinite–coupling–limit Ashkin–Teller model on G^* , such that*

$$Z_{\text{mAT}}(G, G^*; \omega_0, \omega_1, \omega_2, \omega_1) = 2^{-|V^*|+1} \left[\prod_{\langle ij \rangle \in E} \omega_0^* \right] Z_{\text{ICLAT}}(G^*; L_2^*, L_2'^*) \quad (4.19)$$

where the weights couplings $L_2^*, L_2'^*$ are given in terms of the couplings $K_2^*, K_2'^*$ by (4.18).

If we prefer to write the partition function of the mixed AT model as an ICLAT model on G , the procedure is similar: in this case we have to use (4.8) to define the

couplings of the AT model ω_k in terms of those of the mixed AT model $\widehat{\omega}_k$. We obtain (compare to (4.15))

$$\omega_0 = \widehat{\omega}_0 + \widehat{\omega}_1 \quad (4.20a)$$

$$\omega_1 = \widehat{\omega}_0 - \widehat{\omega}_1 \quad (4.20b)$$

$$\omega_2 = \widehat{\omega}_2 + \widehat{\omega}_3 \quad (4.20c)$$

$$\omega_3 = \widehat{\omega}_2 - \widehat{\omega}_3 \quad (4.20d)$$

so that

$$Z_{\text{mAT}}(G, G^*; \widehat{\omega}_0, \widehat{\omega}_1, \widehat{\omega}_2, \widehat{\omega}_3) = Z_{\text{AT}}(G; \omega_0, \omega_1, \omega_2, \omega_3) \quad (4.21)$$

We then notice that $\omega_3 = 0$ if and only if $\widehat{\omega}_2 = \widehat{\omega}_3$, which is in turn equivalent to $\widehat{K}'_2 = \widehat{K}_4$.

But the ratios of weights for this AT mode are precisely the couplings of the ICLAT model:

$$\frac{\omega_1}{\omega_0} = e^{-2K'_2 - 2K_4} = e^{-2L'_2} \quad (4.22a)$$

$$\frac{\omega_2}{\omega_0} = e^{-2K_2 - 2K_4} = e^{-2L_2} \quad (4.22b)$$

In terms of the mixed AT couplings we get that the couplings of the ICLAT model are given by the expressions:

$$e^{-2L'_2} = \frac{\widehat{\omega}_0 - \widehat{\omega}_1}{\widehat{\omega}_0 + \widehat{\omega}_1} = \tanh(2\widehat{K}'_2) \quad (4.23a)$$

$$e^{-2L_2} = \frac{2\widehat{\omega}_2}{\widehat{\omega}_0 + \widehat{\omega}_1} = \frac{e^{-2\widehat{K}_2}}{\cosh(2\widehat{K}'_2)} \quad (4.23b)$$

The above considerations prove the following

Theorem 4.4 *Let $G = (V, E)$ be a planar graph. Then the mixed Ashkin–Teller model (3.24)/(3.25) on G and G^* with equal couplings $K'_2 = K_4$, is equivalent to the infinite–coupling–limit Ashkin–Teller model on G , such that*

$$Z_{\text{mAT}}(G, G^*; \widehat{\omega}_0, \widehat{\omega}_1, \widehat{\omega}_2, \widehat{\omega}_2) = 2^{-|V|+1} \left[\prod_{\langle ij \rangle \in E} \omega_0 \right] Z_{\text{ICLAT}}(G; L_2, L'_2) \quad (4.24)$$

where the weights couplings L_2, L'_2 are given in terms of the couplings $\widehat{K}_2, \widehat{K}'_2$ by (4.23).

4.3 Partial trace transformation

The goal of this section is to show that the HMBW model on various Eulerian plane triangulations can be mapped onto ICLAT models defined on the most common lattices (square, hexagonal, triangular, and kagome). Let us start with the following lemma:

Lemma 4.5 *Let $\sigma_1, \dots, \sigma_{2k}$ take the values ± 1 , and define $\sigma_{2k+1} = \sigma_1$. Then, if $1 \leq k \leq 3$,*

$$\cosh \left[J \sum_{i=1}^{2k} \sigma_i \sigma_{i+1} \right] = \cosh \left[J \sum_{i=1}^k \sigma_{2i} + J \sum_{j=1}^k \sigma_{2j-1} \sigma_{2j} \sigma_{2j+1} \right]. \quad (4.25)$$

Moreover, when $k \geq 4$ this equality does not hold.

PROOF. The statement (4.25) is equivalent to prove that the following quantity $A(k)$ vanishes when all $\sigma_i^2 = 1$, $\sigma_{2k+1} = \sigma_1$, and $1 \leq k \leq 3$:

$$A(k) = \frac{1}{2} \left[\left(\sum_{i=1}^{2k} \sigma_i \sigma_{i+1} \right)^2 - \left(\sum_{i=1}^{2k} \sigma_{2i} + \sum_{j=1}^k \sigma_{2j-1} \sigma_{2j} \sigma_{2j+1} \right)^2 \right]. \quad (4.26)$$

The most direct way to show that $A(k) = 0$ for $k = 1, 2, 3$ when $\sigma_i^2 = 1$ and $\sigma_{2k+1} = \sigma_1$ is to write down the above expression with $t_i = 1 - \sigma_i^2$ and taking into account the latter condition ($\sigma_{2k+1} = \sigma_1$). We arrive easily at the expressions:

$$A(1) = t_1^2(t_2 - 1), \quad (4.27a)$$

$$A(2) = -t_1 t_3 (\sigma_2 + \sigma_4)^2, \quad (4.27b)$$

$$A(3) = - \sum_{j=1}^3 t_{2j-1} [t_{2j+1} t_{2j} - 2\sigma_{2j} \sigma_{2j-2} + 2\sigma_{2j} \sigma_{2j+1} \sigma_{2j-2} \sigma_{2j-3}], \quad (4.27c)$$

where we have explicitly used the identifications $\sigma_{2k+1} = \sigma_1$ and $\sigma_{2k} = \sigma_0$. It is obvious that when $t_i = 0$, then $A(k) = 0$ for $k = 1, 2, 3$.

For $k \geq 4$ (4.26) cannot be true as the first term of the r.h.s. of Eq. (4.26) contains products of up to four spins, while the second term of the r.h.s. of Eq. (4.26) contains products of six spins, and none of them can be simplified using the boundary conditions $\sigma_{2k+1} = \sigma_1$. ■

Remark. Eq. (4.25) can be rewritten as a sum over a spin σ_0 :

$$\sum_{\sigma_0=\pm 1} e^{J \sum_{i=1}^{2k} \sigma_0 \sigma_i \sigma_{i+1}} = \sum_{\sigma_0=\pm 1} \exp \left[J \sum_{i=1}^k \sigma_0 \sigma_{2i} + J \sum_{j=1}^k \sigma_0 \sigma_{2j-1} \sigma_{2j} \sigma_{2j+1} \right]. \quad (4.28)$$

Therefore, a 3-spin Ising model can be written as a certain Ising model with 2- and 4-spin interactions.

The first non-trivial application corresponds to $k = 2$ (see Figure 7). Let us suppose we have an Eulerian plane triangulation $G = (V, E)$, such that $V = V_1 \cup V_2 \cup V_3$, and such that each vertex $i \in V_3$ has degree $\Delta_3 = 4$. (This happens for all the lattices belonging to the family described in Section 2.2.) If we perform

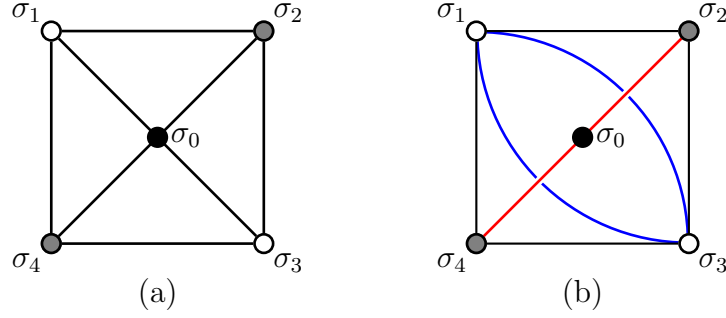


Figure 7: (a) The Ising model with uniform 3-spin interaction $J(\sigma_0\sigma_1\sigma_2 + \sigma_0\sigma_2\sigma_3 + \sigma_0\sigma_3\sigma_4 + \sigma_0\sigma_4\sigma_1)$. (b) The Ising model with 2-spin interaction $J(\sigma_0\sigma_2 + \sigma_0\sigma_4)$, and 4-spin interaction $J(\sigma_0\sigma_1\sigma_2\sigma_3 + \sigma_0\sigma_3\sigma_4\sigma_1)$ obtained from (a) after applying Lemma 4.5 with $k = 2$.

the transformation of Lemma 4.5 to the vertices on V_3 , then the HMBW model on G with coupling constant J (3.1)/(3.2) can be written as a mixed AT model on $G_{13} = (V_1 \cup V_3, E_{13})$, whose dual is $G_{13}^* = (V_2, E_{13}^*)$ [or on $G_{23} = (V_2 \cup V_3, E_{23})$ whose dual is $G_{23}^* = (V_1, E_{23}^*)$]. Both the two-spin coupling $\sigma_i\sigma_j$, and the 4-spin coupling $\sigma_i\sigma_j\sigma_{i^*}\sigma_{j^*}$ (for any $\langle ij \rangle \in E_{13}$) take the same value J ; but the coupling between dual spins is zero. Again, the edge $e^* = \langle i^*j^* \rangle \in E_{13}^*$ is the one *uniquely* associated to the edge $e \in E_{13}$. Notice that the vertices in V_3 (depicted as black dots in Figure 7) subdivide the edge joining the two vertices in V_1 (depicted as gray dots in Figure 7). Therefore, there are two dual edges (depicted as blue curves on Figure 7(b)) joining the two dual vertices in V_2 (depicted as white dots in Figure 7). The Hamiltonian of the transformed system is therefore

$$\mathcal{H} = -J \sum_{\langle ij \rangle \in E_{13}} \sigma_i \sigma_j - J \sum_{\langle ij \rangle \in E_{13}} \sigma_i \sigma_j \sigma_{i^*} \sigma_{j^*} \quad (4.29a)$$

$$= -J \sum_{\langle ij \rangle \in E_{13}} (1 + \sigma_{i^*} \sigma_{j^*}) \sigma_i \sigma_j \quad (4.29b)$$

The relation between partition functions is clear: given an Eulerian plane triangulation $G = (G, V)$, such that $V = V_1 \cup V_2 \cup V_3$, $E = E_{12} \cup E_{13} \cup E_{23}$, and the degree of all vertices in V_3 is $\Delta_3 = 4$, then

$$Z_{\text{HMBW}}(G; J) = Z_{\text{MAT}}(G_{13}, G_{13}^*; J, 0, J), \quad (4.30)$$

where $G_{13} = (V_1 \cup V_3, E_{13})$, and its dual graph is $G_{13}^* = (V_2, E_{13}^*)$.

The $k = 3$ case is shown in Figure 8. Let us suppose we have an Eulerian plane triangulation $G = (V, E)$, such that $V = V_1 \cup V_2 \cup V_3$, and such that each vertex $i \in V_3$ has degree $\Delta_3 = 6$. (This happens for the triangular and bisected-hexagonal lattices.) If we perform the transformation of Lemma 4.5 to the vertices on V_3 , then the HMBW model on G with coupling constant J (3.1)/(3.2) can be written as a

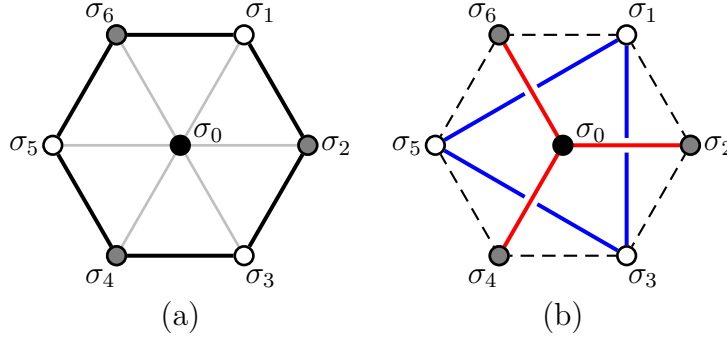


Figure 8: (a) The Ising model with uniform 3-spin interaction $J(\sigma_0\sigma_1\sigma_2 + \sigma_0\sigma_2\sigma_3 + \sigma_0\sigma_3\sigma_4 + \sigma_0\sigma_4\sigma_5 + \sigma_0\sigma_5\sigma_6 + \sigma_0\sigma_6\sigma_1)$. (b) The Ising model with 2-spin interaction $J(\sigma_0\sigma_2 + \sigma_0\sigma_4 + \sigma_0\sigma_6)$, and 4-spin interaction $J(\sigma_0\sigma_1\sigma_2\sigma_3 + \sigma_0\sigma_3\sigma_4\sigma_5 + \sigma_0\sigma_5\sigma_6\sigma_1)$ obtained from (a) after applying Lemma 4.5 with $k = 3$.

mixed AT model on $G_{13} = (V_1 \cup V_3, E_{13})$ [or on $G_{23} = (V_2 \cup V_3, E_{23})$], whose dual graph is $G_{13}^* = (V_2, E_{13}^*)$; and again all couplings are equal to J , except the couplings between dual vertices, which are zero. The model can be written as in (4.29)/(4.30).

We can gather the above results in the following

Theorem 4.6 *Let $G = (V, E)$ be an Eulerian plane triangulation with vertex set $V = V_1 \cup V_2 \cup V_3$, edge set $E = E_{12} \cup E_{13} \cup E_{23}$, and such that the degree of all vertices in V_3 is $\Delta_3 = 4$ or 6 . Then the Hintermann–Merlini–Baxter–Wu model on G (3.1)/(3.2) with coupling constant J is equivalent to a mixed Ashkin–Teller model (3.24)/(3.25) with uniform coupling constant $K_2 = K_4 = J$ and $K'_2 = 0$ on $G_{13} = (V_1 \cup V_3, E_{13})$ [with $G_{13}^* = (V_2, E_{13}^*)$], such that*

$$Z_{\text{HMBW}}(G; J) = Z_{\text{MAT}}(G_{13}, G_{13}^*; J, 0, J). \quad (4.31)$$

(We can equally define the mixed AT model on $G_{23} = (V_2 \cup V_3, E_{23})$, and the formulas are the same after interchanging $1 \leftrightarrow 2$.)

Using Theorem 4.3, we can obtain the following

Corollary 4.7 *Let $G = (V, E)$ be an Eulerian plane triangulation with vertex set $V = V_1 \cup V_2 \cup V_3$, edge set $E = E_{12} \cup E_{13} \cup E_{23}$, and such that the degree of all vertices in V_3 is $\Delta_3 = 4$ or 6 . Then the uniform Hintermann–Merlini–Baxter–Wu model on G (3.1)/(3.2) with coupling constant J is equivalent to an infinite-coupling-limit Ashkin–Teller model (3.15)/(3.16) on $G_{13}^* = (V_2, E_{13}^*)$, where $G_{13} = (V_1 \cup V_3, E_{13})$, and such that*

$$Z_{\text{HMBW}}(G; J) = 2^{-|V_2|+1} Z_{\text{ICLAT}}(G_{13}^*; L_2, L'_2), \quad (4.32)$$

where

$$e^{-2L_2} = \frac{1}{\cosh(2J)} \quad (4.33a)$$

$$e^{-2L'_2} = \tanh(2J) \quad (4.33b)$$

These couplings satisfy

$$\left(e^{-2L_2}\right)^2 + \left(e^{-2L'_2}\right)^2 = 1. \quad (4.34)$$

We can apply this corollary to the main lattices in this paper:

- (a) If G is the triangular lattice and we choose G_{13} to be one of its hexagonal sublattices, then G_{13}^* is the other triangular sublattice. Then, the triangular-lattice HMBW model with coupling J is equivalent to a triangular-lattice ICLAT model with couplings (L_2, L'_2) satisfying the condition (4.34).
- (b) If G is the union-jack lattice and we choose G_{13} to be a decorated square lattice (formed by the degree-4 black vertices and the degree-8 gray vertices in Figure 3(a)), then G_{13}^* is also a square lattice, tilted 45° , formed by the degree-8 white dots in Figure 3(a), and with double edges. Then, the union-jack-lattice HMBW model with coupling J is equivalent to a square-lattice ICLAT model with couplings (L_2, L'_2) satisfying condition

$$e^{-2L'_2} + e^{-2L'_2} = 1, \quad (4.35)$$

because of the double edges.

If G is the bisected-hexagonal lattice, then we have several choices for G_{13} :

- (c) If G_{13} is the decorated triangular lattice formed by the degree-4 and degree-12 vertices in G (black and gray dots, respectively in Figure 3(b)), then G_{13}^* is a hexagonal lattice formed by the degree-6 vertices in G (white dots) and double edges. Then, the bisected-hexagonal-lattice HMBW model with coupling J is equivalent to a hexagonal-lattice ICLAT model with couplings (L_2, L'_2) satisfying the condition (4.35).
- (d) If G_{13} is the hexagonal lattice formed by the degree-4 and degree-6 vertices in G (black and white dots, respectively in Figure 3(b)), then G_{13}^* is a triangular lattice formed by the degree-12 vertices in G (gray dots), and double edges. Then, the bisected-hexagonal-lattice HMBW model with coupling J is equivalent to a triangular-lattice ICLAT model with couplings (L_2, L'_2) satisfying the condition (4.35).
- (e) If G_{13} is the diced lattice formed by the degree-6 and degree-12 vertices in G (white and gray dots, respectively in Figure 3(b)), then G_{13}^* is a kagome lattice formed by the degree-4 vertices in G (black dots). Then, the bisected-hexagonal-lattice HMBW model with coupling J is equivalent to a kagome-lattice ICLAT model with couplings (L_2, L'_2) satisfying the condition (4.34).

In conclusion, the HMBW model on several Eulerian triangulations can be exactly mapped along certain curves ((4.34) or (4.35)) on the ICLAT model defined on other lattices.

Some of these results can be obtained using the decimation transformation (see Appendix A). This latter transformation can be applied in the case $k = 2$ with general couplings J_i ; but reduce to some of the above results in the homogeneous case $J_i = J$.

4.4 Mapping between the BW and two-color non-overlapping Eulerian-bond models

Let us start with a BW model: that is, a HMBW model (3.1)/(3.2) model defined on the triangular lattice $G = (V, E)$. Then, both the vertex and the edge sets can be partitioned into three disjoint sets $V = V_1 \cup V_2 \cup V_3$, and $E = E_{12} \cup E_{13} \cup E_{23}$, so that for all $i \neq j$, E_{ij} contains all edges $e = \langle xy \rangle$ with $x \in V_i$ and $y \in V_j$. Each triangular face $t = \{x, y, z\}$ contains one edge from each set E_{ij} ; therefore, we can rewrite the Hamiltonian (3.1) as

$$\mathcal{H}_{\text{BW}} = -J \sum_{\{i,j\} \in E_{23}} \sigma_i \sigma_j (\sigma_p + \sigma_q), \quad (4.36)$$

where $\{i, j, p\}$ and $\{i, j, q\}$ are only two triangular faces sharing the common edge $e = \langle ij \rangle \in E_{23}$. Notice that the subgraph $(V_2 \cup V_3, E_{23})$ is a hexagonal lattice.

The Boltzmann weight associated to an arbitrary edge $e = \langle ij \rangle \in E_{23}$ can be rewritten as

$$e^{J\sigma_i \sigma_j (\sigma_p + \sigma_q)} = \cosh [J(\sigma_p + \sigma_q)] \{1 + \sigma_i \sigma_j \tanh [J(\sigma_p + \sigma_q)]\}. \quad (4.37)$$

If we now use the trivial identities:

$$\cosh [J(\sigma_p + \sigma_q)] = \frac{\cosh 2J}{(\cosh 2J)^{\delta_{\sigma_p, -\sigma_q}}} = \begin{cases} \cosh 2J & \text{if } \sigma_p = \sigma_q \\ 1 & \text{if } \sigma_p \neq \sigma_q \end{cases} \quad (4.38a)$$

$$\tanh [J(\sigma_p + \sigma_q)] = \sigma_p \delta_{\sigma_p, \sigma_q} \tanh 2J = \begin{cases} \sigma_p \tanh 2J & \text{if } \sigma_p = \sigma_q \\ 0 & \text{if } \sigma_p \neq \sigma_q \end{cases} \quad (4.38b)$$

we can perform a high-temperature expansion of the partition function (3.2)/(4.36):

$$\begin{aligned} Z_{\text{BW}}(G; J) &= (\cosh 2J)^{|E_{23}|} 2^{|V_2 \cup V_3|} \sum_{\substack{\{\sigma_p\} \\ p \in V_1}} \sum_{\substack{E' \subseteq E_{23} \\ E' \text{ Eulerian}}} \prod_{e \in E_{23}} \left(\frac{1}{\cosh 2J} \right)^{\delta_{\sigma_p, -\sigma_q}} \\ &\quad \times \prod_{e \in E'} \sigma_p \delta_{\sigma_p, \sigma_q} \tanh 2J, \end{aligned} \quad (4.39)$$

with E' being the subset of edges in E_{23} contributing with a factor proportional to $\tanh 2J$. Notice that

- (a) The sum over subsets E' only contains Eulerian subgraphs $(V_2 \cup V_3, E')$. Because $(V_2 \cup V_3, E_{23})$ is a hexagonal lattice of maximum degree $\Delta = 3$, the subgraphs that contribute to the partition function (4.39) are precisely the class of non-intersecting Eulerian loops.
- (b) The spins that appear in (4.39) live on the sublattice V_1 . Because of the factor $\sigma_p \delta_{\sigma_p, \sigma_q}$, all spins on any boundary of a loop should be equal.
- (c) Because the hexagonal lattice is bipartite, all loops have even length. Therefore, the factors σ_p in (4.39) cancel out, and always give a contribution equal to 1.

With these considerations (4.39) can be rewritten as

$$\begin{aligned}
Z_{\text{BW}}(G; J) &= (\cosh 2J)^{|E_{23}|} 2^{|V_2 \cup V_3|} \sum_{\substack{E' \subseteq E_{23} \\ E' \text{ Eulerian}}} (\tanh 2J)^{|E'|} \\
&\quad \times \sum_{\substack{\{\sigma_p\} \\ p \in V_1}} \prod_{e \in E_{23}} \left(\frac{1}{\cosh 2J} \right)^{\delta_{\sigma_p, -\sigma_q}} \prod_{e \in E'} \delta_{\sigma_p, \sigma_q}, \quad (4.40)
\end{aligned}$$

The inverse powers of $\cosh 2J$ can be interpreted as contributions from domain-wall loops: i.e., low-temperature loops which separate regions with all spins equal to $+1$ from regions with all spins equal to -1 . Notice that $(\cosh 2J)^{-\delta_{\sigma_p, -\sigma_q}}$ only gives a non-trivial contribution when $\sigma_p \neq \sigma_q$. These low-temperature loops are also non-intersecting, and in addition, they cannot cross any high-temperature loop. See Figure 9 for an example.

In summary, the partition function of the BW model (3.1)/(4.36) is equivalent to a loop gas with the following two conditions: (1) the loops are non-intersecting, and (2) there are two species of loops: the high-temperature loops with weight $\tanh 2J$ per edge, and the low-temperature loops with weight $\cosh^{-1} 2J$ per edge. The partition function can be finally written as

$$Z_{\text{BW}}(G; J) = (2 \cosh 2J)^{|E_{23}|} \sum_{k \geq 0} \sum_{\substack{\text{loops with } k \\ \text{components}}} \prod_{j=1}^k \left\{ (\tanh 2J)^{\ell_j} + \left(\frac{1}{\cosh 2J} \right)^{\ell_j} \right\}, \quad (4.41)$$

where ℓ_j is the length of the j -th loop.

Because $\tanh^2 2J + \cosh^{-2} 2J = 1$, we can parametrize the weights with a single parameter θ :

$$\sin \theta = \frac{1}{\cosh 2J}, \quad \cos \theta = \tanh 2J, \quad (4.42)$$

so that

$$Z_{\text{BW}}(G; J) = (2 \cosh 2J)^{|E_{23}|} \sum_{k \geq 0} \sum_{\substack{\text{loops with } k \\ \text{components}}} \prod_{j=1}^k \{ \sin^{\ell_j} \theta + \cos^{\ell_j} \theta \}. \quad (4.43)$$

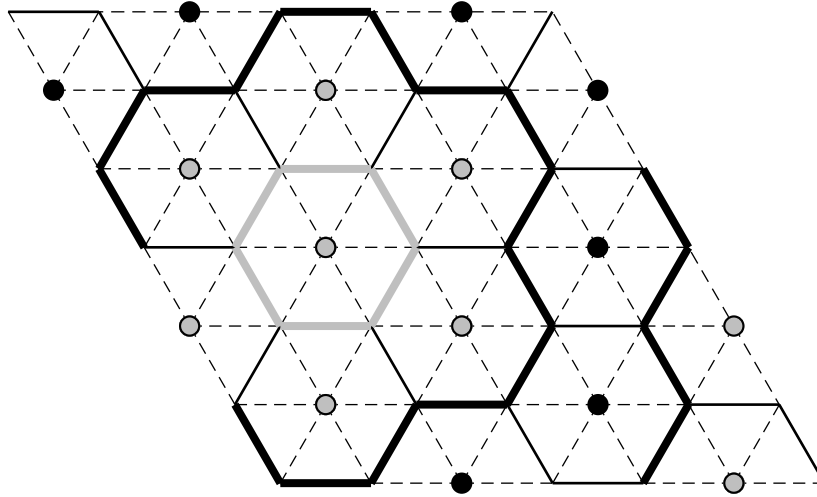


Figure 9: The BW model as a two-color non-overlapping loop model on the hexagonal lattice. We show a finite subset of a triangular lattice $G = (V, E)$. The hexagonal sublattice is formed by the subgraph $(V_2 \cup V_3, E_{23})$; the vertices of this sublattice are not depicted, while the edges are depicted as solid lines. The vertices belonging to the subset V_1 are depicted as dots: a black (resp. gray) dot corresponds to an associated spin taking the value $+1$ (resp. -1). The edges not in E_{23} are depicted as dashed thin lines. The low-temperature loops (depicted as thick black lines) separate regions with opposite spin values. The high-temperature loops (depicted as thick solid gray lines) are surrounded by spins all taking the same value. As this is a finite piece of the triangular lattice, we can only show some parts of the loops.

If we perform a duality transformation in the HMBW model with $J \rightarrow J^*$ ($v \rightarrow 2/v^*$) [13], the loop weights are interchanged: $\tanh 2J \rightarrow \cosh^{-1} 2J^*$, and $\cosh^{-1} 2J \rightarrow \tanh 2J^*$. This agrees with the interpretation of those loops as high-temperature and low-temperature loops. The uniform HMBW model is self-dual when $J = J^*$. In terms of the loop model, we obtain that (4.43) is self-dual at

$$\sin \theta_c = \cos \theta_c = \frac{1}{\sqrt{2}}. \quad (4.44)$$

Notice that the loop model (4.43) is an inhomogeneous $O(2)$ model [24]

$$Z_{O(n)}(\beta_1, \dots, \beta_n) = \sum_{k \geq 0} \sum_{\substack{\text{loops with } k \\ \text{components}}} \prod_{j=1}^k \left(\sum_{\alpha=1}^n \beta_{\alpha}^{\ell_j} \right) \quad (4.45)$$

with weights

$$\beta_1 = \tanh 2J, \quad \beta_2 = \cosh^{-1} 2J. \quad (4.46)$$

This model becomes homogeneous at the self-dual point (4.44), and this self-dual point corresponds to the critical point for the $O(2)$ model [24] on the hexagonal

lattice:

$$\beta_c(n) = \frac{1}{\sqrt{2 + \sqrt{2 - n}}}, \quad (4.47)$$

as

$$\lim_{n \rightarrow 2} \beta_c(n) = \frac{1}{\sqrt{2}} = \tanh 2J_c. \quad (4.48)$$

This is indeed the critical value Baxter and Wu found for the BW model [cf. (3.5b)].

Remarks. 1. It is worth noticing that when $\beta_1 \rightarrow \infty$ and $\beta_2 \rightarrow 0$, we obtain one type of fully packed loops (FPL) [25]. This model is equivalent to a dimer covering of the hexagonal lattice [26], which in turn can be described in the continuum limit by a conformal field theory of central charge $c = 1$ [27, 28]. However, no value of J seems to provide these limiting values.

2. There exists a direct mapping between the ICLAT model and the two-color non-overlapping Eulerian-bond model. The loops correspond to low-temperature graphs (or domain walls) of the two copies of Ising spins. We can rewrite the ICLAT-model partition function (3.16) as

$$\begin{aligned} Z_{\text{ICLAT}}(G; L_2, L'_2) = \sum_{\{\sigma, \tau\}} \prod_{e = \langle ij \rangle \in E} & \left[e^{-2L'_2} \delta_{\sigma_i, \sigma_j} + e^{-2L_2} \delta_{\tau_i, \tau_j} \right. \\ & \left. + \left(1 - e^{-2L'_2} - e^{-2L_2} \right) \delta_{\sigma_i, \sigma_j} \delta_{\tau_i, \tau_j} \right]. \end{aligned} \quad (4.49)$$

Indeed, the weights for each edge coincide with those normalized weights given in the third column of Table 2. One places occupied bonds on the edges of the dual graph G^* as in the standard low-temperature expansion procedure: place an occupied bond of color “A” (resp. color “B”) on the dual edge e^* if the Ising spins τ (resp. σ) on the corresponding original edge $e = \langle ij \rangle$ are not equal, i.e. $\tau_i \tau_j = -1$ (resp. $\sigma_i \sigma_j = -1$). Note that any dual edge cannot be occupied by two bonds of distinct colors, as the configuration $\tau_i \tau_j = \sigma_i \sigma_j = -1$ has zero weight. If G is the triangular lattice, then G^* is the hexagonal lattice, and loops cannot intersect. But for other lattices, loops of distinct colors can intersect at certain vertices. In summary, one obtains a one-to-two correspondence between a two-color non-overlapping Eulerian-bond model on the dual graph G^* , and the ICLAT model on the original graph G .

5 Phase diagrams

In this section we will qualitatively describe the phase diagrams for the ICLAT models defined on the square, triangular, hexagonal, and kagome lattice. We will use the analytic results obtained in the preceding section, as well as exact results from the 8-vertex model [3].

Some important points will be studied using Monte Carlo (MC) simulations. In these cases, we have used the embedding algorithm for the AT model [29] with one difference. In the ferromagnetic regime, in the algorithm of Ref. [29] one fixes one type of spins (either σ or τ) and performs a standard Swendsen-Wang cluster algorithm

[30,31] with the other type. In the simulation for this paper, we fixed one of the *three* types of spins (σ , τ , or $\sigma\tau$). The fixing of the variable $\sigma\tau$ seems important in reducing the critical slowing down for the ICLAT model. For the antiferromagnetic regime, we performed the embedding using the Wang–Swendsen–Kotecký [32] algorithm.

The Binder Q_i cumulants for different observables were computed for each value of the parameters (L_2, L'_2) , and from the crossing of these cumulants for distinct values of the linear size, we extracted the critical values of the parameters. Details will be published elsewhere.

5.1 Square-lattice ICLAT model

In this section we will consider the phase diagram for a square-lattice ICLAT model. It is interesting to start with the phase diagram for the symmetric AT model on the square lattice, as it is simpler than that of the full AT model [33].

First of all, as the square lattice is bipartite, the phase diagram of the symmetric AT on the square lattice should be invariant under the interchange $K_2 \rightarrow -K_2$ [cf. (3.13)]. Thus, we will focus on the part with $K_2 > 0$: See Figure 10.

There are some “easy” points in this phase diagram.

- The line $K_4 = 0$ corresponds to two decoupled Ising models, so there are Ising critical points at $(K_4, K_2) = (0, \pm \frac{1}{2} \log(1 + \sqrt{2}))$. Point DIs in Figure 10 represents the ferromagnetic one (+ sign).
- The line $K_2 = 0$ corresponds to an Ising model in the variable $\sigma\tau$. There are Ising critical points at $(K_4, K_2) = (\pm \frac{1}{2} \log(1 + \sqrt{2}), 0)$. Point Is in Figure 10 represents the ferromagnetic one (+ sign), and point AFIs represents the anti-ferromagnetic one (− sign).
- The limit $K_4 \rightarrow \infty$ corresponds to an Ising model with coupling $2K_2$; therefore, we have Ising critical points at $(K_4, K_2) \rightarrow (\infty, \pm \frac{1}{4} \log(1 + \sqrt{2}))$. The ferromagnetic point (+ sign) is represented by point Is’ in Figure 10.
- The $K_2 = K_4$ subspace corresponds to the 4-state Potts model. This model has a ferromagnetic critical point at $(K_4, K_2) = \frac{1}{4} \log 3$ (point P in Figure 10). The antiferromagnetic 4-state Potts model on the square lattice is disordered even at zero temperature [34,35].

The square lattice is self-dual; therefore the square-lattice AT model is self-dual on the curve (4.13). For the symmetric AT model (3.14), this curve takes the form:

$$e^{-2K_4} = \sinh(2K_2). \quad (5.1)$$

The AT model on any planar graph can be mapped onto an 8-vertex model on the medial graph [20]. In particular, the AT model on the square lattice can be mapped onto a *staggered* 8-vertex model on the square lattice (which has not been solved in general). As a special case, the AT model on the self-dual manifold (4.13) maps onto a *homogeneous* eight-vertex model, which is exactly solvable [3]. Finally,

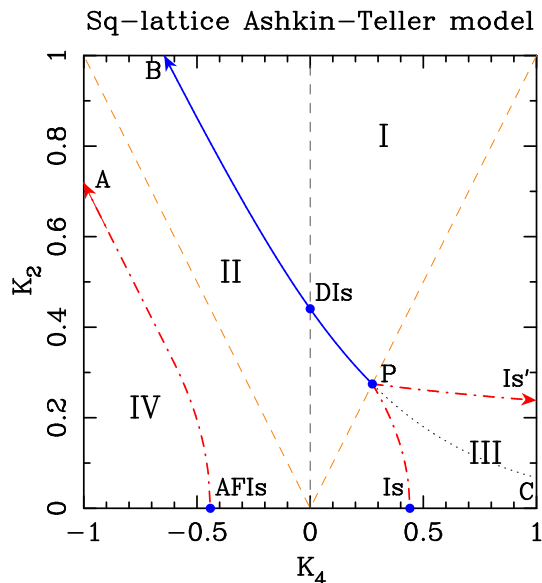


Figure 10: Phase diagram on the square-lattice symmetric AT model (3.14) in the plane (K_4, K_2) . The self-dual curve (5.1) is B–DIIs–P–C. The solid (blue) curves represent the critical part of the self-dual curve, the (red) dot-dashed curves represent Ising-like transition lines, the dashed (orange) lines represent the 4-state Potts subspace, and the dotted curve represents the noncritical part of the self-dual curve (5.1). The Roman numerals designate the different phases of the model (see text).

the symmetric AT model (3.14) on the square lattice maps (after a simple further transformation) onto a *homogeneous* 6-vertex model. In this way, Baxter showed that the self-dual curve (5.1) is critical only for $K_4 \leq \frac{1}{4} \log 3$ (blue solid curve in Figure 10), and it is noncritical for $K_4 > \frac{1}{4} \log 3$ (dotted curve in Figure 10). The critical part can be described by a conformal field theory of central charge $c = 1$ (i.e., it can be related to the Gaussian model). Along this line the critical exponents vary continuously, thus violating the usual notion of universality.

Even though the exact solution of the symmetric square-lattice AT model is not known, we have evidence [36–38] that two critical curves emerge at the 4-state Potts model critical point P: one goes to the Ising critical point Is, and the other one tends as $K_4 \rightarrow \infty$ to the critical Ising point Is'. Finally, there is another critical curve emerging from the Ising critical point AFIs and pointing toward $K_4 \rightarrow -\infty$. The exact location of these three curves is still an open problem, as well as their universality classes. However, it is generally believed that the three curves belong to the Ising universality class.

The phase diagram of this model shows four different phases:

- I. This is the so-called Baxter phase [36]. The spins σ and τ are independently ferromagnetically ordered. There are four extremal infinite-volume Gibbs states, one for each choice for the signs of $\langle \sigma \rangle$ and $\langle \tau \rangle$. The sign of $\langle \sigma \tau \rangle$ is that of $\langle \sigma \rangle \langle \tau \rangle$.

- II. This is the paramagnetic phase, in which the three spins σ , τ , and $\sigma\tau$ are disordered. There is a unique infinite-volume Gibbs state.
- III. In this phase both σ and τ are disordered, but $\sigma\tau$ is ferromagnetically ordered. There are two extremal infinite-volume Gibbs states, one for each choice of the sign of $\langle\sigma\tau\rangle$.
- IV. This is the antiferromagnetic analogue of III: σ and τ are both disordered, but $\sigma\tau$ is antiferromagnetically ordered. There are two extremal infinite-volume Gibbs states.

The critical exponents along the critical part of the self-dual curve can be obtained by relating the AT model to the 8-vertex model or to the Gaussian model [37, 39–42]. We can parametrize the critical part of the self-dual curve (5.1) by using the parameter μ :

$$e^{4K_4} = 1 + 2 \cos \mu, \quad 0 \leq \mu \leq \frac{2\pi}{3}. \quad (5.2)$$

This parameter μ is related to the coupling constant g of the Gaussian model by [42]³

$$\mu = \pi \left(1 - \frac{g}{4}\right), \quad \frac{4}{3} \leq g \leq 4. \quad (5.3)$$

Then, using renormalization-group arguments [37, 39] one finds that the critical exponents along the critical part of the self-dual curve (5.1) are given in terms of μ as

$$\nu = \frac{2 - y}{3 - 2y} \quad (5.4a)$$

$$\alpha = \frac{2 - 2y}{3 - 2y} \quad (5.4b)$$

$$\beta = \frac{2 - y}{8(3 - 2y)} \quad (5.4c)$$

$$\gamma = \frac{7(2 - y)}{4(3 - 2y)} \quad (5.4d)$$

$$\beta' = \frac{1}{4(3 - 2y)} \quad (5.4e)$$

$$\gamma' = \frac{7 - 4y}{2(3 - 2y)} \quad (5.4f)$$

where y is the renormalization-group eigenvalue related to μ via

$$y = \frac{2\mu}{\pi}, \quad 0 \leq y \leq \frac{4}{3}, \quad (5.5)$$

³ Our g is that of Saleur [42] and equals 2π times of the K of Kadanoff and Brown [39], and Yang [41].

and the magnetic exponents β, γ (resp. β', γ') correspond to the σ or τ (resp. $\sigma\tau$) magnetization. The value of the critical exponents (5.4) vary along the self-dual curve (5.1); but there are two exponents that remain constant on this curve

$$\eta = 2 - \frac{\gamma}{\nu} = \frac{1}{4} \quad (5.6a)$$

$$\delta = 1 + \frac{\gamma}{\beta} = 15 \quad (5.6b)$$

Finally, it is worth commenting that the AT domain walls (considered as extended curves) have also critical exponents (of the watermelon type). This has recently been investigated by Picco and Santachiara [43, 44], and by Ikhlef and Rajabpour [21].

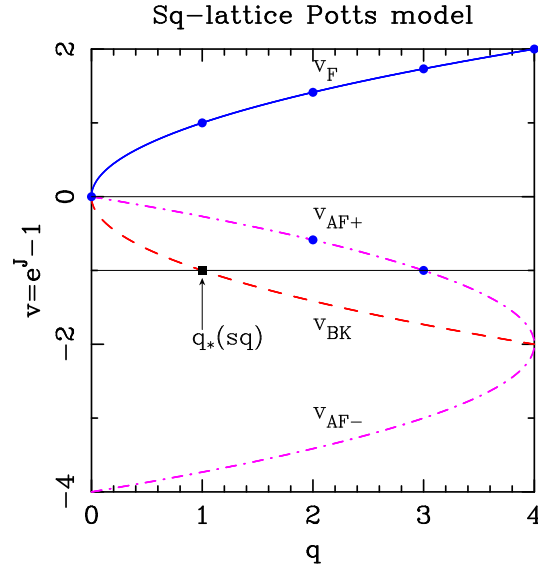


Figure 11: Phase diagram on the square-lattice q -state Potts model in the plane (q, v) , where v is related to the coupling constant J by (5.7). The upper solid (blue) curve $v_F = +\sqrt{q}$ corresponds to the ferromagnetic critical curve. Its continuation (depicted as a dashed – red – curve) corresponds to the BK line $v_{BK} = -\sqrt{q}$. The other two branches $v_{AF+} = -2 + \sqrt{4-q}$ and $v_{AF-} = -2 - \sqrt{4-q}$ correspond respectively to the critical antiferromagnetic and its dual counterpart curves. The dots \bullet represent the critical values of the model for integer values of q . The square \blacksquare represents the intersection of the BK curve $v_{BK} = -\sqrt{q}$ with the zero-temperature limit in the antiferromagnetic regime $v = -1$: i.e. the point $q_*(sq) = 1$.

There is a nice relation between the symmetric square-lattice AT model on the self-dual curve (5.1) and the ferromagnetic q -state Potts model at its critical temperature [45]. Figure 11 shows the phase diagram of the q -state Potts model in the plane (q, v) ,

where v is given in terms of the Potts model coupling constant J_{Potts} by⁴

$$v = e^{J_{\text{Potts}}} - 1. \quad (5.7)$$

There are four curves where the exact free energy is known [3, 46]:

$$v = \pm\sqrt{q} \quad (5.8a)$$

$$v = -2 \pm \sqrt{4-q} \quad (5.8b)$$

The curve (5.8a₊) $v_F(q) = \sqrt{q}$ is known to correspond to the ferromagnetic critical point for this model, and it is self-dual. Its analytic continuation into the Berker–Kadanoff (BK) phase [47–49] corresponds to the BK curve (5.8a₋) $v_{\text{BK}}(q) = -\sqrt{q}$, and it is also self-dual. Curve (5.8b₊) $v_{\text{AF}+}(q) = -2 + \sqrt{4-q}$ is expected to give the critical curve for the antiferromagnetic model; in particular, it gives the exactly known values of the critical temperature for $q = 2, 3$. This curve is dual to the curve (5.8b₋) $v_{\text{AF}-}(q) = -2 - \sqrt{4-q}$. The curves $v_{\text{AF}\pm}$ bound the BK phase. The renormalization group flow is repulsive close to this boundary, and it is attracted by the curve v_{BK} lying in between. This curve intersects the line $v = -1$ (corresponding to the zero-temperature Potts model in the antiferromagnetic regime) at a point $q_*(\text{sq}) = 1$.

The above mentioned relation between these two models stems from the fact that both models can be written as six-vertex models [3]. Thus, we can use q to parametrize the critical part of the self-dual curve (5.1). Indeed, this q should be interpreted as an *effective* number of states.⁵ The result is

$$\sqrt{q} = 2 \cos \mu, \quad q \in [0, 4], \quad (5.9)$$

where μ is related to the AT couplings via (5.1)/(5.2).

The critical 4-state Potts model corresponds to $\mu = 0$, $y = 0$, $g = 4$, and $\sqrt{q} = 2$ (point P in Figure 10); the two decoupled Ising models correspond to the point $\mu = \pi/2$, $y = 1$, $g = 2$, and $\sqrt{q} = 0$ (point DIs in Figure 10). The part of the AT self-dual curve connecting these two models ($y \leq 1$) is characterized by $\alpha \geq 0$, and corresponds to going from $q = 4$ down to $q = 0$ along the ferromagnetic critical curve v_F . Therefore, $0 \leq \mu \leq \pi/2$ corresponds to the Potts-model critical curve v_F .

If we keep moving to higher values of μ (i.e., $2\pi/3 \leq \mu \leq \pi/2$), then we enter the BK branch v_{BK} . This corresponds to $y > 1$, and $\sqrt{q} < 0$. In particular, the specific heat is not divergent in this regime (i.e., $\alpha < 0$), as the energy is *not* a relevant operator in the BK phase. We can move down the curve v_{BK} until we enter the unphysical regime of the Potts model: i.e., $v = -1$, which corresponds to the zero-temperature limit of the *antiferromagnetic* Potts model. We expect that this point

⁴ We have used the same letter as for the temperature-like variable in the HMBW model (3.4). It should be clear from the context which v we are referring to.

⁵ Please note that this not imply that the AT and Potts models are equivalent. The AT model is untwisted, so that (unlike the Potts model) the central charge is $c = 1$ throughout the critical regime.

q_* is lattice-dependent, as universality usually does not hold in the antiferromagnetic regime. This limiting point along the self-dual curve (5.1) as $K_4 \rightarrow -\infty$ (point B in Figure 10) corresponds to $\mu = 2\pi/3$, $y = 4/3$, $g = 4/3$, and $\sqrt{q} = -1$. Its universality class is characterized by the following critical exponents (5.4):

$$\nu = 2, \quad \alpha = -2, \quad \beta = \frac{1}{4}, \quad \beta' = \frac{3}{4}, \quad \gamma = \frac{7}{2}, \quad \gamma' = \frac{5}{2}, \quad (5.10)$$

and the two critical exponents η and δ as in (5.6).

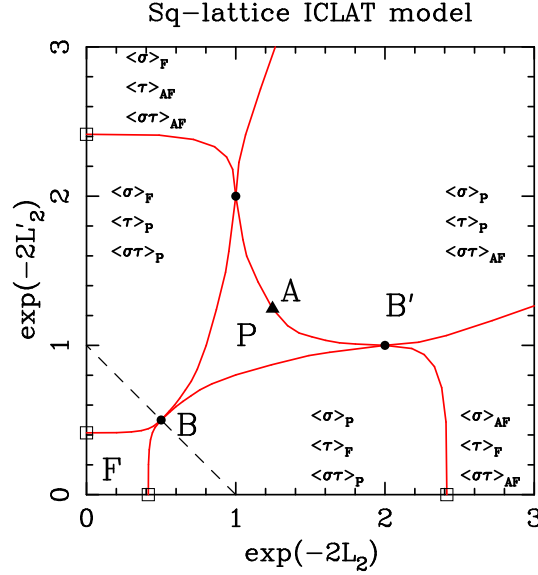


Figure 12: Phase diagram on the square-lattice ICLAT model (3.15) in the plane $(e^{-2L_2}, e^{-2L'_2})$. The (red) solid curves are Ising-like critical curves, except at the dots of coordinates $(1/2, 1/2)$, $(1, 2)$, and $(2, 1)$. Point B of coordinates $(1/2, 1/2)$ corresponds to the point where the self-dual curve of the symmetric AT model (5.1) hits this plane, and the other two points are equivalent to the former one due to the symmetries of this model. All these points are depicted as solid circles (\bullet). Point A (\blacktriangle) shows where the branch emerging from point AFIs in Figure 10 hits the ICLAT model. The dashed curve going through point B corresponds to the union-jack HMWB model subspace (4.35). The squares (\square) on the axes correspond to the exact Ising critical points located at $\sqrt{2} \pm 1$. The distinct phases are denoted by the ordering of the distinct spins: e.g., $\langle \sigma \rangle_P$, $\langle \tau \rangle_F$, and $\langle \sigma \tau \rangle_{AF}$ means respectively, that the σ spins are disordered, the τ spins are ferromagnetically ordered, and that the product $\sigma \tau$ is antiferromagnetically ordered. F corresponds to the ferromagnetic phase: $\langle \sigma \rangle_F$, $\langle \tau \rangle_F$, $\langle \sigma \tau \rangle_F$; and P corresponds to the paramagnetic phase: $\langle \sigma \rangle_P$, $\langle \tau \rangle_P$, $\langle \sigma \tau \rangle_P$.

Let us now consider the square-lattice ICLAT model. Its phase diagram is shown

in Figure 12, and it is symmetric under the interchange $L_2 \leftrightarrow L'_2$ because of (3.18). Therefore, we will focus on the part with $L'_2 \geq L_2$.

First of all, we want to know where the self-dual curve (5.1) hits the plane $(e^{-2L_2}, e^{-2L'_2})$ in the limit $K_4 \rightarrow -\infty$. We can rewrite (5.1) as

$$e^{-2(K_2+K_4)} = \frac{1}{2} (1 - e^{-4K_2}) \rightarrow \frac{1}{2}, \quad (5.11)$$

in the limit $K_4 \rightarrow -\infty$ and $K_2 = K'_2 \rightarrow +\infty$, with $K_2 + K_4 = L_2$ and $K'_2 + K_4 = L'_2 = L_2$ held fixed. Thus, the self-dual curve (5.1) hits the ICLAT model at the symmetric point

$$(e^{-2L_2}, e^{-2L'_2}) = \left(\frac{1}{2}, \frac{1}{2}\right). \quad (5.12)$$

This point is depicted as B in Figure 12, and it is equivalent to point B' of coordinates

$$(e^{-2L_2}, e^{-2L'_2}) = (2, 1), \quad (5.13)$$

because of the symmetry (3.22).

Remark. Ikhlef and Rajabpour [21, Section 4] have consider the square-lattice ICLAT model at the symmetric point (5.11)/(5.12). They found that at this particular point, this ICLAT model can be mapped onto an integrable 19-vertex model. Furthermore, they also mapped this particular point of the square-lattice ICLAT model onto an integrable dilute Brauer model.

In the limit $L'_2 \rightarrow \infty$, we have a square-lattice Ising model on the σ spins. Therefore, we have the following two critical points:

$$(e^{-2L_2}, e^{-2L'_2}) = (\sqrt{2} \pm 1, 0), \quad (5.14)$$

where the '+' (resp. '-') sign corresponds to the antiferromagnetic (resp. ferromagnetic) Ising critical point. Using (3.22), we see that these two points are mapped to points at infinity with slopes $\sqrt{2} \mp 1$. All these points belong to the Ising universality class.

The point $L_2 = L'_2 = 0$ corresponds to a zero-temperature 4-state Potts antiferromagnet. This model is disordered on the square lattice. Therefore, the point

$$(e^{-2L_2}, e^{-2L'_2}) = (1, 1) \quad (5.15)$$

belongs to the paramagnetic phase, which is indicated with the sign P in Figure 12.

The point $L_2 = L'_2 \rightarrow +\infty$ corresponds to a zero-temperature point in the ferromagnetic regime; therefore, the region around the origin in the $(e^{-2L_2}, e^{-2L'_2})$ plane corresponds to a ferromagnetically ordered phase, denoted by F in Figure 12.

We know from Section 4.3, that the union-jack-lattice HMBW model with coupling J is equivalent to an ICLAT model on the square lattice on the line (4.35). This line is depicted as a (black) dashed line in Figure 12. Indeed, the self-dual point for this HMBW model corresponds to the critical point (5.12).

Baxter has shown that the AT model on the square lattice can be mapped onto a *staggered* eight-vertex model on the square lattice [3], with weights (a, b, c, d) on one sublattice, and weights (a, b, d, c) on the other sublattice. These weights can be written (up to some unimportant multiplicative constant) in terms of the parameters L_2, L'_2 of the square-lattice ICLAT model as follows (see [3, Eqs. (12.9.6) and (12.9.17)]):

$$a = \omega_0 + \omega_1 = 1 + e^{-2L'_2} \quad (5.16a)$$

$$b = \omega_2 - \omega_3 = e^{-2L_2} \quad (5.16b)$$

$$c = \omega_2 + \omega_3 = e^{-2L_2} \quad (5.16c)$$

$$d = \omega_0 - \omega_1 = 1 - e^{-2L'_2} \quad (5.16d)$$

where the weights ω_k correspond to the ICLAT model, and can be read from the third column of Table 2. The above staggered eight-vertex model becomes *homogeneous* when $c = d$. In terms of the couplings L_2, L'_2 , this implies that the model should satisfy (4.35). The vertex weights (5.16) reduce along this line to

$$a = 2 - e^{-2L_2} \quad (5.17a)$$

$$b = c = d = e^{-2L_2} \quad (5.17b)$$

In order to characterize the different phases, it is useful to compute the parameter Δ :

$$\Delta \equiv \frac{a^2 + b^2 - c^2 - d^2}{2(ab + cd)} = e^{2L_2} - 1 \quad (5.18)$$

When $0 \leq e^{-2L_2} < \frac{1}{2}$, we have that $\Delta > 1$ and hence, the eight-vertex model is ordered (it belongs to the ferroelectric Regime I in Baxter's notation [3], as $a > b + c + d$). On the other hand, when $e^{-2L_2} > \frac{1}{2}$, we have that $|\Delta| < 1$, and the system is disordered (it belongs to Baxter's Regime III). Thus, there is a critical point at the symmetric point (5.12).

In order to obtain the value of the parameter μ at this critical point, we first need to make use of the rearrangement procedures explained in Baxter's book [3, Section 10.11], so that the transformed weights (a_r, b_r, c_r, d_r) belong to Baxter's principal regime IV (the anti-ferroelectric phase with $c > a + b + c$ and $\Delta < -1$). To achieve this, we first use the duality (or weak-graph) transformation [3, Eq. (10.2.5)]:

$$a' = \frac{1}{2}(a + b + c + d) = 1 + e^{-2L_2} \quad (5.19a)$$

$$b' = \frac{1}{2}(a + b - c - d) = 1 - e^{-2L_2} \quad (5.19b)$$

$$c' = \frac{1}{2}(a - b + c - d) = 1 - e^{-2L_2} \quad (5.19c)$$

$$d' = \frac{1}{2}(a - b - c + d) = 1 - e^{-2L_2} \quad (5.19d)$$

so that the model with weights (a', b', c', d') belongs to the ferroelectric regime I ($a' > b' + c' + d'$ with $\Delta > 1$). Then, we make the change $(a_r, b_r, c_r, d_r) = (c', d', a', b')$,

so that the model now belongs to the principal regime. The critical value of the parameter μ is given in terms of the weights (a_r, b_r, c_r, d_r) when $e^{-2L_2} = 1/2$:

$$\tan \frac{\mu}{2} = \sqrt{\frac{c_r d_r}{a_r b_r}} = \sqrt{3}, \quad (5.20)$$

and hence,

$$\mu = \frac{2\pi}{3}. \quad (5.21)$$

In this case, the critical exponents are those of the eight-vertex model for the same value of μ [3, Equations (10.12.24)/(10.12.25)]:

$$\nu = \frac{1}{y} \quad (5.22a)$$

$$\alpha = 2 - \frac{2}{y} \quad (5.22b)$$

$$\beta = \frac{1}{8y} \quad (5.22c)$$

$$\gamma = \frac{7}{4y} \quad (5.22d)$$

$$\beta' = \frac{2-y}{4y} \quad (5.22e)$$

$$\gamma' = \frac{2+y}{2y} \quad (5.22f)$$

where y is given by (5.5). The numerical values for these exponents at the symmetric point (5.12) are:

$$\nu = \frac{3}{4}, \quad \alpha = \frac{1}{2}, \quad \beta = \frac{3}{32}, \quad \beta' = \frac{1}{8}, \quad \gamma = \frac{21}{16}, \quad \gamma' = \frac{5}{4}. \quad (5.23)$$

These results agree with the result found by Hintermann and Merlini [2]: the self-dual point (3.5) of the union-jack-lattice HMBW model is critical with critical exponent $\alpha = 1/2$.

We find that, on one hand, the value of $\mu = 2\pi/3$ at the symmetric point $e^{-2L_2} = e^{-2L'_2} = 1/2$ is the same, independently of how we approach that point, either along the self-dual curve (5.1) when $K_4 \rightarrow -\infty$, or along the HMBW-model line (4.35). However, we get two different sets of critical exponents: if we follow the self-dual curve (5.1), we should use the expressions (5.4) obtained by renormalization-group arguments; but along the line (4.35), one should use instead the eight-vertex exponents (5.22).

The exponents $1/\nu = 1/2$ in Eq. (5.10) and $1/\nu = 4/3$ in Eq. (5.23) correspond to the renormalization exponents along the diagonal direction (i.e. along the self-dual curve in the large-coupling limit) in Figure 10, and the perpendicular-to-diagonal direction (i.e., along the dashed line in Figure 12), respectively. The same behavior will be found in the triangular and hexagonal lattices (see the next two sections).

Finally, all points (except point B and its symmetric counterparts) on the solid curves in Figure 12 belong to the Ising universality class. We have checked this fact numerically by computing via MC simulations the values of the critical exponents on several points on these curves.

5.2 Triangular-lattice ICLAT model

The phase diagram for the symmetric AT model on the triangular lattice is qualitatively different from that for the square lattice. The main reason is that the triangular lattice is not bipartite; therefore, there is no symmetry $K_2 \rightarrow -K_2$. However, if we focus on the ferromagnetic regime $K_2 \geq 0$, then it is rather similar, except that phase IV does not exist. See [50] for a recent study of this model.

Another difference with respect to the same model on the square lattice is that the symmetric AT model on the triangular lattice is not self-dual, and it does not satisfy in general the star-triangle equation. However, it does satisfy the star-triangle equation on a certain curve in the (K_2, K_4) plane. Temperley and Ashley [51] found that this curve is given by

$$e^{-4K_4} = \frac{1}{2}(e^{4K_2} - 1) \quad (5.24)$$

The qualitative behavior of the symmetric triangular-lattice AT model on this curve is similar to that for the square lattice:

- The model is critical only for $K_4 \leq \frac{1}{4} \log 2$, and it can be mapped onto the Gaussian model with central charge $c = 1$.
- At $K_4 = K_2 = \frac{1}{4} \log 2$, the critical curve splits into two Ising-like critical curves. This point corresponds to the critical coupling for a ferromagnetic 4-state Potts model on the triangular lattice.
- For $K_4 > \frac{1}{4} \log 2$, the curve is no longer critical.

One of the Ising-like critical curves emerging at $K_4 = K_2 = \frac{1}{4} \log 2$ goes to the Ising critical point at $(K_2, K_4) = (0, \frac{1}{4} \log 3)$. The other line goes to the Ising critical point at $K_4 \rightarrow \infty$ with $K_2 = \frac{1}{2} \log 3$.

As the subspace $K_2 = 0$ corresponds to an Ising model in the variables $\sigma\tau$, then we expect the above ferromagnetic critical point at $K_4 = \frac{1}{4} \log 3$, and an antiferromagnetic critical point in the limit $K_4 \rightarrow -\infty$. Thus, there is no AFIs-A curve, like in the phase diagram for the square lattice (see Figure 10).

Finally, the 4-state antiferromagnetic Potts model on the triangular lattice has a zero-temperature critical point. This point is recovered when $K_2 = K_4 \rightarrow -\infty$.

We expect that the same critical exponents will be found for the part of the curve (5.24) between the critical points for the 4-state Potts and the two decoupled Ising models. The effective number of Potts states along the curve (5.24) is given by [51, Equation (18)]:

$$\sqrt{q} = \sqrt{2} \frac{e^{2K_2}(3 - e^{4K_2})}{(e^{4K_2} - 1)^{3/2}}, \quad (5.25)$$

and again the relation between q and μ is given by (5.9). Then, the 4-state Potts critical point is defined by $e^{4K_2} = 2$; hence, $q = 4$ and $\mu = 0$. The decoupled Ising models are obtained for $e^{4K_2} = 3$, and thus, $q = 0$ and $\mu = \pi/2$. These values of q , and μ indeed agree with those obtained for the square-lattice AT model, as we expect universality to hold in the ferromagnetic regime.

However, when we take larger values of $\mu > \pi/2$, we enter the BK curve v_{BK} for the triangular lattice [49]. This is the middle branch of the curve [45, 52, 53]

$$v^3 + 3v^2 = q, \quad (5.26)$$

and hits the $v = -1$ line at $q_{*}(\text{tri}) = 2$. This corresponds to $\sqrt{q} = -\sqrt{2}$, $\mu = 3\pi/4$, and $y = 3/2$. These values differ from those of the square-lattice model, and lead to a different set of critical exponents for this point:

$$\nu = \infty, \quad \frac{\alpha}{\nu} = -2, \quad \frac{\beta}{\nu} = \frac{1}{8}, \quad \frac{\beta'}{\nu} = \frac{1}{2}, \quad \frac{\gamma}{\nu} = \frac{7}{4}, \quad \frac{\gamma'}{\nu} = 1. \quad (5.27)$$

Saleur [42] indicates that at this point $\mu = 3\pi/4$ or $g = 1$ one has a Kosterlitz-Thouless transition. In Refs. [54, 55] the values for α/ν , γ/ν , and β/ν in (5.27) were obtained by studying the critical $O(2)$ loop model on the hexagonal lattice. It is interesting to note that the triangular-lattice Ising $q = 2$ antiferromagnet at zero temperature $v = -1$ is critical with $c = 1$.

Let us now consider the triangular-lattice ICLAT model. Its phase diagram is given in Figure 13. Again it is symmetric under the interchange $L_2 \leftrightarrow L'_2$, so we will focus on the subspace $L'_2 \geq L_2$.

First of all we would like to compute the symmetric point in the $(e^{-2L_2}, e^{-2L'_2})$ space where the critical curve (5.24) ends. This is easily obtained from (5.24) if we take $K_4, -K_2 \rightarrow -\infty$ with $K_2 + K_4 = L_2 = L'_2$ fixed. The result is

$$(e^{-2L_2}, e^{-2L'_2}) = \left(\frac{1}{\sqrt{2}}, \frac{1}{\sqrt{2}} \right). \quad (5.28)$$

This corresponds to point B in Figure 13.

Some important particular cases are given by

- $e^{-2L'_2} = 0$ corresponds to an Ising model on the σ variables. Thus, there are phase transitions at

$$e^{-2L_2} = \frac{1}{\sqrt{3}} \quad (5.29a)$$

$$e^{-2L_2} = +\infty \quad (5.29b)$$

The first solution corresponds to the ferromagnetic Ising critical point; while the second one is the antiferromagnetic critical point at zero temperature.

- The triangular-lattice HMBW model (or simply the BW model) [4, 5, 56] corresponds to the circle (4.34). For $e^{-2L_2} > \frac{1}{\sqrt{2}}$ the model is disordered, for $e^{-2L_2} < \frac{1}{\sqrt{2}}$, the model is ordered, and finally at $e^{-2L_2} = \frac{1}{\sqrt{2}}$, the model is critical.

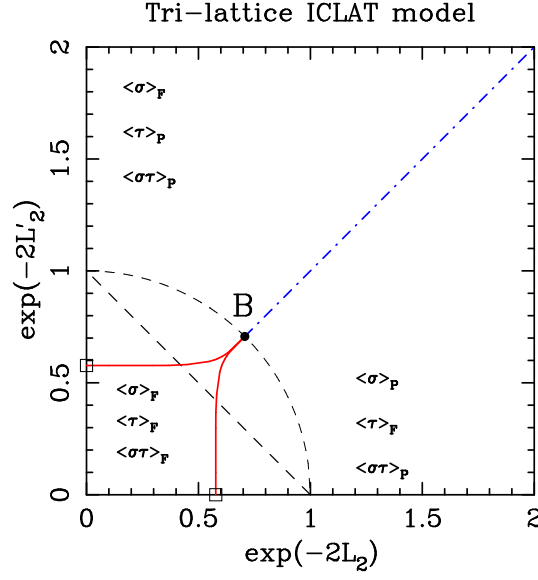


Figure 13: Phase diagram on the triangular-lattice ICLAT model (3.15) in the plane $(e^{-2L_2}, e^{-2L'_2})$. Point B (depicted as a black dot) has coordinates $(1/\sqrt{2}, 1/\sqrt{2})$, and corresponds to the point where the self-dual curve of the symmetric AT model (5.24) hits this plane. The ferromagnetic Ising critical point for $e^{-2L'_2} = 0$ is located at $e^{-2L_2} = 1/\sqrt{3}$. The dashed arc going through point B corresponds to the triangular-lattice HMBW model, and the dashed line joining $(0, 1)$ and $(1, 0)$ corresponds to the bisected-hexagonal-lattice HMBW model. The notation for curves, symbols, and phases is as in Figure 12. The main diagonal starting at point B (depicted as a blue dot-dashed line) corresponds to a line of critical points belonging to the same universality class as point B.

- In Section 4.3, we showed that the bisected-hexagonal-lattice HMBW model corresponds to the line (4.35).

Wu [20] suggested that the triangular AT model should correspond to a *uniform* 8-vertex model on the kagome lattice. The details were worked out by Temperley and Ashley [51]. Theorem 4.1 tells us that the triangular-lattice AT model with weights $\{\omega_k\}$ is equivalent to a mixed AT model on the triangular and hexagonal lattices with weights $\{\hat{\omega}_k\}$ given by (4.8). Then, Theorem 4.4 relates this mixed AT model with couplings $\{\hat{K}_2, \hat{K}'_2, \hat{K}_4\}$, with an ICLAT model on the triangular lattice with couplings $\{L_2, L'_2\}$ given by (4.23). Notice that we have $\omega_3 = 0$ in the triangular-lattice AT model, so that $\hat{\omega}_2 = \hat{\omega}_3$ in the mixed AT model, which also means that the couplings for this model satisfy $\hat{K}'_2 = \hat{K}_4$.

We also know by following Wu [20] that this mixed AT model can be related to an 8-vertex model on the medial of the triangular lattice (i.e., a kagome lattice) with

weights

$$a = \hat{\omega}_0 = \frac{\omega_0 + \omega_1}{2} = e^{\hat{K}_2 + 2\hat{K}'_2} \quad (5.30a)$$

$$b = \hat{\omega}_3 = \frac{\omega_2 - \omega_3}{2} = e^{-\hat{K}_2} \quad (5.30b)$$

$$c = \hat{\omega}_2 = \frac{\omega_2 + \omega_3}{2} = e^{-\hat{K}_2} \quad (5.30c)$$

$$d = \hat{\omega}_1 = \frac{\omega_0 - \omega_1}{2} = e^{\hat{K}_2 - 2\hat{K}'_2} \quad (5.30d)$$

where we have taken into account that $\hat{K}'_2 = \hat{K}_4$. Baxter [3] found that this uniform 8-vertex model on the kagome lattice can be solved by transforming it to a square-lattice 8-vertex model when the following condition is fulfilled⁶

$$\frac{d}{a} = \frac{c^2 - d^2}{a^2 - b^2}. \quad (5.31)$$

When $b = c$ [cf. (5.30)], this condition implies that $ad = b^2$, or equivalently, $\hat{K}_2 = 0$. Therefore, the 8-vertex model on the kagome lattice is soluble by Baxter's methods if the weights have the form:

$$a = e^{2\hat{K}'_2} \quad (5.32a)$$

$$b = c = 1 \quad (5.32b)$$

$$d = e^{-2\hat{K}'_2} \quad (5.32c)$$

This 8-vertex model is critical if $a = b + c + d$. This equation implies that

$$\sinh(2\hat{K}'_2) = 1 \quad \Leftrightarrow \quad e^{-2L_2} = e^{-2L'_2} = \frac{1}{\sqrt{2}}. \quad (5.33)$$

This corresponds to the symmetric point (5.28).

To obtain the value of μ corresponding to this point, we proceed as for the square lattice. If $e^{-2L_2} > 1/\sqrt{2}$, the model is disordered (it belongs to regime III). Using the weak-graph transformation (5.19), we can get a point in regime I with weights:

$$a' = 1 + \cosh 2\hat{K}'_2 \quad (5.34a)$$

$$b' = c' = \sinh 2\hat{K}'_2 \quad (5.34b)$$

$$d' = -1 + \cosh 2\hat{K}'_2 \quad (5.34c)$$

⁶ Notice we have followed Wu's notation [20] to go from spin configurations to arrow configurations, and this choice is non-equivalent to that of Baxter [3] or Temperley–Ashley [51]. We can “translate” Baxter's formulas to our notation by using the transformation $(a, b, c, d) \rightarrow (c, d, a, b)$.

If we do the transformation $(a', b', c', d') \rightarrow (c', d', a', b') = (a_r, b_r, c_r, d_r)$, we get finally into the principal regime, with weights

$$a_r = d_r = \sinh 2\hat{K}'_2 \quad (5.35a)$$

$$b_r = -1 + \cosh 2\hat{K}'_2 \quad (5.35b)$$

$$c_r = 1 + \cosh 2\hat{K}'_2 \quad (5.35c)$$

Using these weights, we compute the critical value of μ :

$$\tan \frac{\mu}{2} = \sqrt{\frac{c_r d_r}{a_r b_r}} = \sqrt{2} + 1, \quad (5.36)$$

and hence,

$$\mu = \frac{3\pi}{4}. \quad (5.37)$$

The numerical values for these exponents at the symmetric point (5.28) are:

$$\nu = \frac{2}{3}, \quad \alpha = \frac{2}{3}, \quad \beta = \frac{1}{12}, \quad \beta' = \frac{1}{12}, \quad \gamma = \frac{7}{6}, \quad \gamma' = \frac{7}{6}. \quad (5.38)$$

These results agree with the result found by Baxter and Wu [4, 5, 56].

It is worth noticing that these exponents coincide with those for the ferromagnetic 4-state Potts model $\mu = 0$. In fact, these two models are believed to belong to the same universality class [6]. One striking difference between the BW model and the 4-state Potts model is that the latter displays logarithmic corrections (both multiplicative and additive) [8–10], while the former does not have any of these.

A qualitative phase diagram for this model is shown in Figure 13. We expect, as in the square-lattice case, that at the point B (where the self-dual curve of the symmetric AT model hits the ICLAT plane), the critical curve splits into two curves going to Ising-like critical points on the axis. These curves are expected to be Ising-like. We also know that the line (4.35) corresponds to the HMBW model on the bisected-hexagonal lattice. The phase diagram shows that this model has *two* critical points, contrary to what we know about the same model on the other two triangulations (triangular and union-jack lattices). Our numerical MC results show that their location is:⁷

$$e^{2L_2} = 0.4196(15), \quad e^{2L'_2} = 0.5803(8) \quad (5.39a)$$

$$e^{2L_2} = 0.5803(8), \quad e^{2L'_2} = 0.4196(15) \quad (5.39b)$$

In terms of the HMBW coupling J (4.33), we obtain the critical points

$$J_{1,c} = 0.5003(5), \quad J_{2,c} = 0.3857(4). \quad (5.40)$$

Indeed, we can check that these two values are mutually dual: using the definition (3.4), we arrive at $v_1 v_2 = 2.001(3)$. Therefore, we suggest the following:

⁷ We performed the MC computation on the kagome lattice (see section 5.4). The values of the couplings for the triangular lattice are the square of those obtained for the kagome lattice.

Conjecture 5.1 *The Hintermann–Merlini–Baxter–Wu model (3.1)/(3.2) on the bisected-hexagonal lattice has two critical points*

$$J_{1,c} = \frac{1}{2}, \quad J_{2,c} = \frac{1}{2} \log \left(\frac{e+1}{e-1} \right) \approx 0.3859684164. \quad (5.41)$$

These two points are mutually dual.

Finally, the diagonal line starting at point B and depicted as a dot-dashed line on Figure 13 belongs to the same universality class as point B. This is supported by our MC simulations along this line. The above statement is true for all points on this diagonal line, except in the limit $e^{L_2} = e^{L'_2} \rightarrow +\infty$, where we recover a hexagonal-lattice FPL model with fugacity $n = 2$. This FPL model is equivalent to the zero-temperature limit of the triangular-lattice 4-state Potts antiferromagnet [57, 58]. Therefore, its continuum limit can be described by a conformal field theory of central charge $c = 2$ [25].

5.3 Hexagonal-lattice ICLAT model

The phase diagram for the symmetric AT model on the hexagonal lattice is qualitatively the same as for the square lattice, as both lattices are bipartite. However, the AT model on the hexagonal lattice is not self-dual; but it does satisfy the star-triangle equation on a certain curve in the (K_2, K_4) plane. Temperley and Ashley [51] found that this curve is given by

$$e^{-4K_4} + e^{-2K_4} \cosh 2K_2 = \sinh^2 2K_2 \quad (5.42)$$

We then find that

- The model is critical only for $K_4 \leq \frac{1}{4} \log 5$, and it can be mapped onto the Gaussian model with central charge $c = 1$.
- At $K_4 = K_2 = \frac{1}{4} \log 5$, the critical curve splits into two Ising-like critical curves. This point corresponds to the critical coupling for a ferromagnetic 4-state Potts model on the hexagonal lattice.
- For $K_4 > \frac{1}{4} \log 5$, the curve is no longer critical.

As the subspace $K_2 = 0$ corresponds to an Ising model in the variables $\sigma\tau$, then we expect the above ferromagnetic critical point at $K_4 = \frac{1}{2} \log(2 + \sqrt{3})$, and an antiferromagnetic critical point at $K_4 = -\frac{1}{2} \log(2 + \sqrt{3})$. There is a curve of Ising-like critical points emerging from this point, and going to $K_4 \rightarrow -\infty$, as for the square lattice.

Finally, the 4-state antiferromagnetic Potts model on the hexagonal lattice is disordered at all temperatures [59, 60], thus none of the above critical curves cross the line $K_2 = -K_4 \geq 0$.

We expect that the same critical exponents will be found for the part of the curve (5.42) between the critical points for the 4-state Potts and the two decoupled Ising

models. The effective number of Potts states along the curve (5.42) could be obtained from the results given in Ref. [51]:

$$\sqrt{q} = \sqrt{1 + \xi(K_2)} [\xi(K_2) - 2], \quad (5.43)$$

where $\xi(K_2)$ is given by

$$\xi(K_2) = \frac{1}{2 \tanh^2(2K_2)} \left[1 + \sqrt{1 + 4 \tanh^2(2K_2)} \right]. \quad (5.44)$$

Again the relation between q and μ is given by (5.9). Then, the 4-state Potts critical point is defined by $e^{2K_2} = \sqrt{5}$; hence, $\xi = 3$, $q = 4$ and $\mu = 0$. The decoupled Ising models are obtained for $e^{2K_2} = 2 + \sqrt{3}$, and thus, $\xi = 2$, $q = 0$ and $\mu = \pi/2$. These values of q , and μ indeed agree with those obtained for the square-lattice AT model, as we expect universality to hold in the ferromagnetic regime.

When we take larger values of $\mu > \pi/2$, we enter the BK curve v_{BK} for the hexagonal lattice. This is the lower branch of the curve [45, 52, 53]

$$v^3 - 3vq = q^2, \quad (5.45)$$

and hits the $v = -1$ line at $q_*(\text{hex}) = (3 - \sqrt{5})/2$. This corresponds to $\sqrt{q} = (1 - \sqrt{5})/2$, $\mu = 3\pi/5$, and $y = 6/5$. This value coincides with the one we obtain when we take the limit $K_2 \rightarrow +\infty$ in (5.43), as $\lim_{K_2 \rightarrow \infty} \xi(K_2) = (1 + \sqrt{5})/2$. These values lead to the following set of critical exponents for this point:

$$\nu = \frac{4}{3}, \quad \alpha = -\frac{2}{3}, \quad \beta = \frac{1}{6}, \quad \beta' = \frac{5}{12}, \quad \gamma = \frac{7}{3}, \quad \gamma' = \frac{11}{6}. \quad (5.46)$$

Let us now consider the hexagonal-lattice ICLAT model. Its phase diagram is given in Figure 14. Again it is symmetric under the interchange $L_2 \leftrightarrow L'_2$, so we will focus on the subspace $L'_2 \geq L_2$.

First of all we would like to compute the symmetric point in the $(e^{-2L_2}, e^{-2L'_2})$ space where the critical curve (5.42) ends. This is easily obtained from (5.42) if we take $K_4, -K_2 \rightarrow -\infty$ with $K_2 + K_4 = L_2 = L'_2$ fixed. The result is

$$(e^{-2L_2}, e^{-2L'_2}) = \left(\frac{\sqrt{5} - 1}{4}, \frac{\sqrt{5} - 1}{4} \right). \quad (5.47)$$

This corresponds to point B in Figure 14, and it is equivalent to point B' of coordinates

$$(e^{-2L_2}, e^{-2L'_2}) = (1 + \sqrt{5}, 1), \quad (5.48)$$

because of the symmetry (3.22).

Some important particular cases are given by

- $e^{-2L'_2} = 0$ corresponds to an Ising model on the σ variables. Thus, there are phase transitions at

$$e^{-2L_2} = 2 \pm \sqrt{3}. \quad (5.49)$$

The '+' solution corresponds to the ferromagnetic Ising critical point; while the '-' solution is the antiferromagnetic critical point. Symmetry (3.22) implies that these points are mapped to points at infinity with slopes $2 \pm \sqrt{3}$.

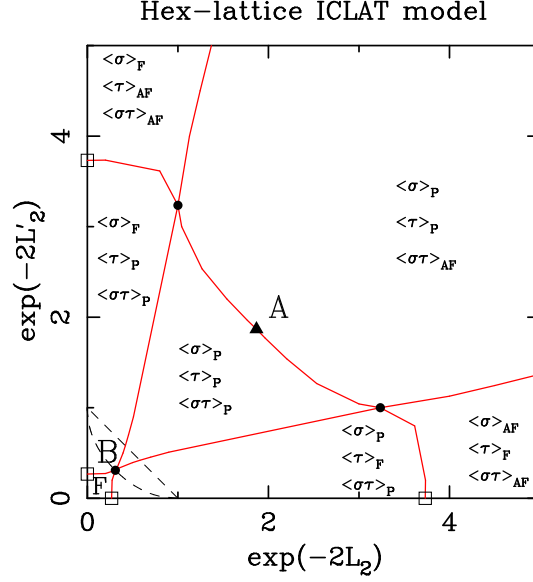


Figure 14: Qualitative phase diagram on the hexagonal-lattice ICLAT model (3.15) in the plane $(e^{-2L_2}, e^{-2L'_2})$. Point B of coordinates $((\sqrt{5}-1)/4, (\sqrt{5}-1)/4)$ corresponds to the point where the self-dual curve of the symmetric AT model (5.42) hits this plane, and the other two points are equivalent to the former one because of the symmetries of this model. The ferromagnetic and antiferromagnetic Ising critical points for $e^{-2L'_2} = 0$ are located at $2 \pm \sqrt{3}$, respectively. The dashed arc going through point B corresponds to the models that are solvable using Baxter's method. The dashed line corresponds to the uniform HMBW model on the bisected-hexagonal lattice. The notation for curves, symbols, and phases is as in Figure 12.

- The point $(e^{-2L_2}, e^{-2L'_2}) = (1, 1)$ corresponds to the zero-temperature 4-state antiferromagnetic Potts model on the hexagonal lattice. This model is known to be disordered [59, 60].
- In Section 4.3, we showed that the bisected-hexagonal-lattice HMBW model corresponds to the line (4.35). In agreement with Conjecture 5.1, we find two critical points on this line at the same values as for the triangular-lattice ICLAT model (5.39) (recall that in Section 4.3 we obtain maps from the bisected-hexagonal-lattice HMBW model to the ICLAT model on *decorated* triangular or hexagonal lattices).

The kagome lattice is also the medial of the hexagonal, thus we can repeat the same argument to relate the hexagonal-lattice ICLAT model to the kagome-lattice 8-vertex model [51], using a mixed AT model as the intermediate step [20]. Again, Theorem 4.1 tells us that the hexagonal-lattice AT model with weights $\{\omega_k\}$ is equivalent to a mixed AT model on the hexagonal and triangular lattices with weights $\{\widehat{\omega}_k\}$ [cf. (4.8)], and this latter model is related to a hexagonal-lattice ICLAT model with

couplings $\{L_2, L'_2\}$ [cf. (4.23)]. Notice that we have $\omega_3 = 0$ in the hexagonal-lattice AT model, so that $\widehat{\omega}_2 = \widehat{\omega}_3$ in the mixed AT model, which also means that the couplings for this model satisfy $\widehat{K}'_2 = \widehat{K}_4$.

The results of Wu [20] ensure that this mixed AT model can be related to an 8-vertex model on the medial of the hexagonal lattice (i.e., a kagome lattice) with weights given by (5.30).

The only difference with respect to the triangular-lattice case is that in this latter case, the σ spins live on the triangular lattice, and the τ spins on the dual hexagonal lattice; while for the hexagonal-lattice case, the situation is reversed: the σ spins live on the hexagonal lattice, and the τ spins live on the dual triangular lattice. This implies that the condition for the corresponding kagome-lattice 8-vertex model to be soluble by Baxter's method now reads:⁸

$$\frac{c}{a} = \frac{d^2 - c^2}{a^2 - b^2}. \quad (5.50)$$

When $b = c$ [cf. (5.30)], this condition implies that the couplings \widehat{K}_2 and \widehat{K}'_2 should satisfy the following equation:

$$x^3 e^{2\widehat{K}'_2} - x^2 e^{4\widehat{K}'_2} - x e^{6\widehat{K}'_2} + 1 = 0, \quad (5.51)$$

where

$$x = e^{-2\widehat{K}_2}. \quad (5.52)$$

It is difficult to write the solutions of the above equation (5.51) as simple expressions in the ICLAT couplings L_2 and L'_2 . However, it is not difficult to prove that the following points provide solutions of (5.51):

$$\left(e^{-2L_2}, e^{-2L'_2}\right) = (1, 0) \quad (5.53a)$$

$$\left(e^{-2L_2}, e^{-2L'_2}\right) = \left(\frac{\sqrt{5}-1}{4}, \frac{\sqrt{5}-1}{4}\right) \quad (5.53b)$$

Therefore, the symmetric point (5.47) belongs to this curve where the ICLAT model is soluble as a 8-vertex model on the square lattice.

Furthermore, the symmetric point (5.47) is the only one where the 8-vertex model is critical. The condition for this 8-vertex model to be critical is

$$a = b + c + d, \quad (5.54)$$

which in terms of the couplings $\widehat{K}_2, \widehat{K}'_2$ means that

$$\sinh 2\widehat{K}'_2 = e^{-2\widehat{K}_2}. \quad (5.55)$$

⁸ Again, we have followed Wu's notation [20] to go from spin configurations to arrow configurations. We can "translate" Baxter's formulas to our notation by using the transformation $(a, b, c, d) \rightarrow (d, c, a, b)$.

This condition implies that

$$e^{-2L'_2} = \tanh 2\hat{K}_2 = e^{-2L_2}. \quad (5.56)$$

Therefore, the model is critical precisely at the symmetric point (5.47).

To obtain the value of μ corresponding to this point, we proceed as for the triangular lattice. By rearranging the weights appropriately so that the model is mapped to the principal regime, we obtain for the value of μ at the critical point (5.47)

$$\tan \frac{\mu}{2} = \sqrt{\frac{5 + 2\sqrt{5}}{5}}, \quad (5.57)$$

and hence,

$$\mu = \frac{3\pi}{5}. \quad (5.58)$$

The numerical values for these exponents at the symmetric point (5.47) are:

$$\nu = \frac{5}{6}, \quad \alpha = \frac{1}{3}, \quad \beta = \frac{5}{48}, \quad \beta' = \frac{1}{6}, \quad \gamma = \frac{35}{24}, \quad \gamma' = \frac{4}{3}. \quad (5.59)$$

Again we find that this set of critical exponents do not agree with the set (5.46) obtained by following the critical curve of the self-dual curve of the hexagonal-lattice symmetric AT model.

Finally, as for the square lattice, we find numerically in our MC simulations that all solid curves in Figure 14 are Ising-like, except point B and its symmetric counterparts.

5.4 Kagome-lattice ICLAT model

The phase diagram for the symmetric AT model on the kagome lattice is expected to be qualitatively similar to that of the same model on the triangular lattice. The main reason is that both lattices are not bipartite. Unfortunately, the exact location of any of the critical curves is unknown for this case. See Ref. [50] for a recent study.

What is exactly known about the behavior of the symmetric kagome-lattice AT model on this curve reduces to the solution of the Ising model [61]:

- For $K_2 = 0$, it is critical in the ferromagnetic regime at coupling

$$K_4 = \frac{1}{4} \log(3 + 2\sqrt{3}). \quad (5.60)$$

- In the antiferromagnetic regime it is always disordered.

Finally, the 4-state Potts model on the kagome lattice has a ferromagnetic critical point at $K_2 = K_4 \approx 0.2873$, and in the antiferromagnetic regime, it is always disordered.

Let us now consider the kagome-lattice ICLAT model. Its phase diagram is given in Figure 15. Again it is symmetric under the interchange $L_2 \leftrightarrow L'_2$, so we will focus on the subspace $L'_2 \geq L_2$.

The position of the critical point on the symmetric subspace is not exactly known for this model. Our numerical MC results show that this point has coordinates $(0.45411(3), 0.45411(3))$. This corresponds to point B in Figure 15.

Some important particular cases are given by

- $e^{-2L'_2} = 0$ corresponds to an Ising model on the σ variables. Thus, there are phase transitions at

$$e^{-2L_2} = \frac{1}{\sqrt{3+2\sqrt{3}}}. \quad (5.61)$$

- In Section 4.3, we showed that the uniform bisected-hexagonal-lattice HMBW model corresponds to the circle (4.34). In agreement with Conjecture 5.1, we find that the critical curve for the kagome-lattice ICLAT model crosses the above circle at *two* points:

$$e^{2L_2} = 0.6478(5), \quad e^{2L'_2} = 0.7618(3) \quad (5.62a)$$

$$e^{2L_2} = 0.7618(3), \quad e^{2L'_2} = 0.6478(5) \quad (5.62b)$$

Indeed, the values of the HMBW coupling J are the same as in (5.40).

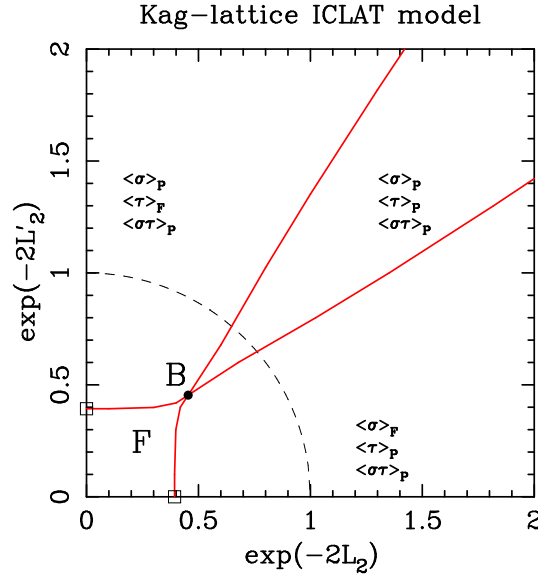


Figure 15: Phase diagram on the kagome-lattice ICLAT model (3.15) in the plane $(e^{-2L_2}, e^{-2L'_2})$. Point B has coordinates $(0.45411(3), 0.45411(3))$, and corresponds to the point where the self-dual curve of the symmetric AT model hits this plane. The ferromagnetic Ising critical point for $e^{-2L'_2} = 0$ is located at $e^{-2L_2} = 0.39360791$. The dashed arc corresponds to the bisected-hexagonal-lattice HMBW model. The notation for curves, symbols, and phases is as in Figure 12.

6 Discussion

The main goal of this paper is the study of the infinite-coupling-limit Ashkin–Teller model on several common lattices, namely, square, triangular, hexagonal, and kagome. We also have considered a generalization of the well-known Baxter–Wu model: the Hintermann–Merlini–Baxter–Wu model defined on any plane Eulerian triangulation.

We have first investigated the relations between these two models. As a side effect we have also considered the Ashkin–Teller and the mixed Ashkin–Teller models, which are known in the literature. In particular we find that

- The partition functions for the AT model on a graph G (3.6) and the mixed AT model (3.25) on G and its dual G^* are equal (modulo some unimportant multiplicative factors):

$$Z_{\text{AT}}(G; \omega_0, \omega_1, \omega_2, \omega_3) \propto Z_{\text{mAT}}(G, G^*; \widehat{\omega}_0, \widehat{\omega}_1, \widehat{\omega}_2, \widehat{\omega}_3),$$

where the weights $\widehat{\omega}_k$ are given in terms of the weights ω_k by (4.8). (See Theorem 4.1.) As a side effect, we recover the duality relation for the AT model (4.12). (See Theorem 4.2.)

- The partition function for the ICLAT model on a graph G (3.16) and the partition function of the mixed AT model (3.25) on G and G^* are again equal (modulo some unimportant multiplicative factors):

$$Z_{\text{mAT}}(G, G^*; \widehat{\omega}_0, \widehat{\omega}_1, \widehat{\omega}_2, \widehat{\omega}_2) \propto Z_{\text{ICLAT}}(G; L_2, L'_2)$$

where the weights couplings L_2, L'_2 are given in terms of the couplings $\widehat{K}_2, \widehat{K}'_2$ (or the weights $\widehat{\omega}_k$) by (4.23). (See Theorem 4.3.)

- Using the partial-trace transformation (Lemma 4.5) we obtain that the HMBW model on certain lattices is a subspace of the ICLAT on other lattices. In particular Corollary 4.7 implies:
 - The triangular-lattice HMBW is equivalent to a triangular-lattice ICLAT model on the subspace (4.34).
 - The bisected-hexagonal-lattice HMBW is equivalent to a kagome-lattice ICLAT model on the subspace (4.34).
 - The union-jack-lattice HMBW is equivalent to a square-lattice ICLAT model on the subspace (4.35).
 - The bisected-hexagonal-lattice HMBW is equivalent to a hexagonal-lattice ICLAT model on the subspace (4.35).
 - The bisected-hexagonal-lattice HMBW is equivalent to a triangular-lattice ICLAT model on the subspace (4.35).

- We have found in Section 4.4 that the partition function for the BW model (i.e., the triangular-lattice HMBW model (3.2)) can be written as a partition function of a 2-color–non-overlapping Eulerian bond model on a hexagonal lattice with weights (4.46).

The second important result is the computation of the phase diagram of the ICLAT model on the square, triangular, hexagonal, and kagome lattices. In the first three cases, we know the exact point (labeled B in the figures) where the self-dual curve of the corresponding symmetric AT model hits the ICLAT model in the limit of infinite couplings. Using the expression for the critical exponents of the symmetric AT along this self-dual curve, we are able to make predictions about the critical exponents at B. On the other hand, in the ICLAT plane, we can also use the relation between the AT model (and its infinite-coupling limit) and the 8-vertex model. From this relation another set of critical exponents arise. In the case of the square and triangular lattice, these predictions agree with the results of Hintermann–Merlini [2] and Baxter–Wu [4,5]. It is interesting to note that these two sets of critical exponents do *not* coincide.

Finally, the exact location of the self-dual curve of the kagome-lattice AT model is not known. In this case, we have obtained a high-precision Monte Carlo estimate for the positions of point B and of the two points where the critical curves cross the bisected-hexagonal HMBW subspace. From these latter values, we have determined the two critical points of the bisected-hexagonal-lattice HMBW model (see Conjecture 5.1).

A Decimation transformation

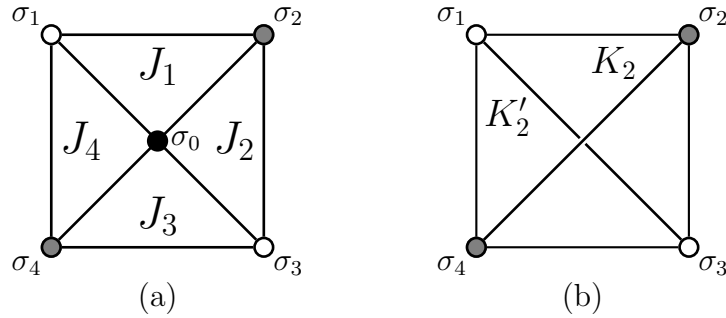


Figure 16: (a) The HMBW model with generic 3-spin interaction $J_1\sigma_0\sigma_1\sigma_2 + J_2\sigma_0\sigma_2\sigma_3 + J_3\sigma_0\sigma_3\sigma_4 + J_4\sigma_0\sigma_4\sigma_1$. (b) The AT model with 2-spin interaction $K_2\sigma_2\sigma_4 + K'_2\sigma_1\sigma_3$, and 4-spin interaction $K_4\sigma_1\sigma_2\sigma_3\sigma_4$ obtained from (a) after summing over the values of $\sigma_0 = \pm 1$.

In this appendix we will consider the decimation transformation, that can be

considered as a generalization of the $k = 2$ case of the partial-trace transformation dealt with in Section 4.3.

Let us suppose we have a general (i.e., face-dependent coupling) HMBW model defined on an Eulerian plane triangulation $G = (V, E)$. Then the vertex set has a tripartition $V = V_1 \cup V_2 \cup V_3$. Let us further suppose that the vertices belonging to the sublattice V_3 have all degree $\Delta_3 = 4$. Then, this general HMBM model can be transformed into a mixed AT model by performing the sum over all spins living on V_3 . (See Figure 16.)

$$\begin{aligned} \sum_{\sigma_0=\pm 1} \exp [\sigma_0 (J_1 \sigma_1 \sigma_2 + J_2 \sigma_2 \sigma_3 + J_3 \sigma_3 \sigma_4 + J_4 \sigma_4 \sigma_1)] \\ = 2 \exp [K_0 + K_2 \sigma_2 \sigma_4 + K_2' \sigma_1 \sigma_3 + K_4 \sigma_1 \sigma_2 \sigma_3 \sigma_4] . \end{aligned} \quad (\text{A.1})$$

Inspecting all the possible configurations for the spins σ_i with $i = 1, 2, 3, 4$, one has the following 4 independent equations

$$\omega_0 = \exp(K_0 + K_2 + K_2' + K_4) = \cosh(J_1 + J_2 + J_3 + J_4) \quad (\text{A.2a})$$

$$\omega_1 = \exp(K_0 - K_2 + K_2' - K_4) = \cosh(J_1 + J_2 - J_3 - J_4) \quad (\text{A.2b})$$

$$\omega_2 = \exp(K_0 + K_2 - K_2' - K_4) = \cosh(J_1 - J_2 - J_3 + J_4) \quad (\text{A.2c})$$

$$\omega_3 = \exp(K_0 - K_2 - K_2' + K_4) = \cosh(J_1 - J_2 + J_3 - J_4) \quad (\text{A.2d})$$

These equations have the solution:

$$\begin{aligned} e^{4K_0} &= \cosh(J_1 + J_2 + J_3 + J_4) \cosh(J_1 + J_2 - J_3 - J_4) \\ &\quad \times \cosh(J_1 - J_2 - J_3 + J_4) \cosh(J_1 - J_2 + J_3 - J_4) \end{aligned} \quad (\text{A.3a})$$

$$e^{4K_2} = \frac{\cosh(J_1 + J_2 + J_3 + J_4) \cosh(J_1 - J_2 - J_3 + J_4)}{\cosh(J_1 + J_2 - J_3 - J_4) \cosh(J_1 - J_2 + J_3 - J_4)} \quad (\text{A.3b})$$

$$e^{4K_2'} = \frac{\cosh(J_1 + J_2 + J_3 + J_4) \cosh(J_1 + J_2 - J_3 - J_4)}{\cosh(J_1 - J_2 - J_3 + J_4) \cosh(J_1 - J_2 + J_3 - J_4)} \quad (\text{A.3c})$$

$$e^{4K_4} = \frac{\cosh(J_1 + J_2 + J_3 + J_4) \cosh(J_1 - J_2 + J_3 - J_4)}{\cosh(J_1 + J_2 - J_3 - J_4) \cosh(J_1 - J_2 - J_3 + J_4)} \quad (\text{A.3d})$$

Notice that the 2-spin terms couple spins placed on the diagonal; not nearest-neighbor ones. Therefore, we obtain a mixed AT model on the graph $G_1 = (V_1, E_1)$ [defined by the vertices in V_1], and its dual $G_1^* = (V_2, E_1^*)$ [defined by the vertices in V_2]:

$$Z_{\text{HMBW}}(G; \mathbf{J}) = 2^{|V_3|} Z_{\text{mAT}}(G_1, G_1^*; \mathbf{K}_2, \mathbf{K}_2', \mathbf{K}_4) \quad (\text{A.4a})$$

$$= 2^{|V_3|} Z_{\text{mAT}}(G_1, G_1^*; \boldsymbol{\omega}_0, \boldsymbol{\omega}_1, \boldsymbol{\omega}_2, \boldsymbol{\omega}_3) \quad (\text{A.4b})$$

where the relation between the mixed AT couplings and the original HMBW couplings is given in (A.3), and the weights $\boldsymbol{\omega}_k$ are given in (A.2). To emphasize that the couplings are face- or edge-dependent, we use boldface letters. The relation between general HMBW, AT, and mixed AT models can be generalized easily from the

mappings discussed in Section 4. Indeed, we can interchange V_1 and V_2 in the above discussion.

We can rewrite (A.4) in terms of the partition function of an AT model on G_1^* by using (4.10):

$$Z_{\text{HMBW}}(G; \mathbf{J}) = 2^{|V_3| - |V_2| + 1} Z_{\text{AT}}(G_1^*; \hat{\omega}_0, \hat{\omega}_2, \hat{\omega}_1, \hat{\omega}_3), \quad (\text{A.5})$$

where the new weights are given by

$$\hat{\omega}_0 = \omega_0 + \omega_2 = 2 \cosh(J_1 + J_2) \cosh(J_3 + J_4) \quad (\text{A.6a})$$

$$\hat{\omega}_1 = \omega_0 - \omega_2 = 2 \sinh(J_1 + J_2) \sinh(J_3 + J_4) \quad (\text{A.6b})$$

$$\hat{\omega}_2 = \omega_1 + \omega_3 = 2 \cosh(J_1 - J_2) \cosh(J_3 - J_4) \quad (\text{A.6c})$$

$$\hat{\omega}_3 = \omega_1 - \omega_3 = 2 \sinh(J_1 - J_2) \sinh(J_3 - J_4) \quad (\text{A.6d})$$

The most interesting case corresponds to a homogeneous HMBW model (3.1)/(3.2) with coupling J . Then, (A.5) reduces to a ICLAT model:

$$Z_{\text{HMBW}}(G; J) = 2^{|V_3| - |V_2| + 1} Z_{\text{AT}}(G_1^*; 2 \cosh^2(2J), 2 \sinh^2(2J), 2, 0) \quad (\text{A.7a})$$

$$= Z_{\text{ICLAT}}(G_1^*; L_2, L'_2) \quad (\text{A.7b})$$

where the couplings L_2, L'_2 are given by:

$$e^{-2L_2} = \frac{1}{\cosh^2(2J)} \quad (\text{A.8a})$$

$$e^{-2L'_2} = \tanh^2(2J) \quad (\text{A.8b})$$

Indeed, the uniform HMBW model on an Eulerian planar triangulation G maps into the line (4.35) of the ICLAT model on the graph G_1^* .

If we apply this transformation to the union-jack lattice we get case (b) of Section 4.3; while if we apply it to the bisected-hexagonal lattice, we obtain cases (c) and (d) of Section 4.3.

Acknowledgments

We wish to warmly thank Tim Garoni, Alan Sokal, and Andrea Sportiello for their collaboration at early stages of this work.

J.S. is grateful to the kind hospitality of the Department of Physics of New York University, and the Hefei National Laboratory for Physical Sciences at Microscale and Department of Modern Physics of the University of Science and Technology of China, where part of this work was done.

The research of Y.H. and Y.D. is supported by National Nature Science Foundation of China under grants No. 11275185 and 10975127, and the Chinese Academy of Sciences. The work of J.L.J. was supported by the Agence Nationale de la Recherche (grant ANR-10-BLAN-0414: DIME), and the Institut Universitaire de France. The research of J.S. was supported in part by Spanish MEC grants FPA2009-08785 and MTM2011-24097 and by U.S. National Science Foundation grant PHY-0424082.

References

- [1] L. Onsager, Phys. Rev. **65**, 117 (1944).
- [2] A. Hintermann and D. Merlini, Phys. Lett. **41A**, 208 (1972).
- [3] R.J. Baxter, *Exactly Solved Models in Statistical Mechanics* (Academic Press, London–New York, 1982).
- [4] R.J. Baxter and F.Y. Wu, Phys. Rev. Lett. **31**, 1294 (1973).
- [5] R.J. Baxter and F.Y. Wu, Aust. J. Phys. **27**, 357 (1974).
- [6] E. Domany and E.K. Riedel, J. Appl. Phys. **49**, 1315 (1978).
- [7] R.B. Potts, Proc. Camb. Phil. Soc. **48**, 106 (1952).
- [8] M. Nauenberg and D.J. Scalapino, Phys. Rev. Lett. **44**, 837 (1980).
- [9] J.L. Cardy, M. Nauenberg and D.J. Scalapino, Phys. Rev. B **22**, 2560 (1980).
- [10] J. Salas and A.D. Sokal, J. Stat. Phys. **88**, 567 (1997), [arXiv:hep-lat/9607030].
- [11] L.N. Shchur and W. Janke, Nucl. Phys. B **840**, 491 (2010), [arXiv:1007.1838].
- [12] D. Merlini and C. Gruber, J. Math. Phys. **13**, 1814 (1972).
- [13] C. Gruber, A. Hintermann, and D. Merlini, *Group Analysis of Classical Lattice Systems*. Lecture Notes in Physics, Vol. 60 (Springer-Verlag, Berlin–Heidelberg–New York, 1977).
- [14] J. Ashkin and E. Teller, Phys. Rev. **64**, 178 (1943).
- [15] C. Fan, Phys. Lett. **39A**, 136 (1972).
- [16] R. Diestel, *Graph Theory* (Springer–Verlag, Heidelberg, New York, 2005).
- [17] M.–T. Tsai and D.B. West, Ars Math. Contemp. **4**, 73 (2011).
- [18] Y. Deng, Y. Huang, J.L. Jacobsen, J. Salas, and A.D. Sokal, Rev. Phys. Lett. **107**, 150601 (2011) [5 pages], [arXiv:1108.1743].
- [19] B. Grünbaum and G.C. Shepard, *Tilings and Patterns* (W.H. Freeman and Company, New York, 1987).
- [20] F.Y. Wu, J. Math. Phys. **18**, 611 (1977).
- [21] Y. Ikhlef and M.A. Rajabpour, J. Stat. Mech., P01012, (2012) [arXiv:1111.3197].
- [22] C. Fan, Phys. Rev. B **6**, 902 (1972).
- [23] F.Y. Wu and Y.K. Wang, J. Math. Phys. **17**, 4439 (1976).

- [24] B. Nienhuis, Phys. Rev. Lett. **49**, 1062 (1982).
- [25] J. Kondev, J. de Gier, and B. Nienhuis, J. Phys. A **29**, 6489 (1996) [cond-mat/9603170].
- [26] P.W. Kasteleyn, J. Math. Phys. **4**, 287 (1963).
- [27] M.E. Fisher and J. Stephenson, Phys. Rev. **132**, 1411 (1963).
- [28] F.Y. Wu, Int. J. Mod. Phys. B **20**, 5357 (2006), [arXiv:cond-mat/0303251].
- [29] J. Salas and A.D. Sokal, J. Stat. Phys. **85**, 297 (1996), [arXiv:hep-lat/9511022].
- [30] R.H. Swendsen and J.S. Wang, Phys. Rev. Lett. **58**, 2 (1987).
- [31] D. Kandel, R. Ben-Av, and E. Domany, Phys. Rev. Lett. **65**, 941 (1990).
- [32] J.S. Wang, R.H. Swendsen, and R. Kotecký, Phys. Rev. Lett. **63**, 109 (1989).
- [33] F.Y. Wu and K.Y. Lin, J. Phys. C **7**, L181 (1974).
- [34] S.J. Ferreira and A.D. Sokal, J. Stat. Phys. **96**, 461 (1999), [arXiv:cond-mat/9811345].
- [35] J. Salas and A.D. Sokal, J. Stat. Phys. **92**, 729 (1998), [arXiv:cond-mat/9801079].
- [36] R.V. Ditzian, J.R. Banavar, G.S. Grest, and L.P. Kadanoff, Phys. Rev. B **22**, 2542 (1980).
- [37] H.J.F. Knops, Ann. Phys. (N.Y.) **128**, 448 (1980).
- [38] G. Kamieniarz, P. Kozłowski, and R. Dekeyser, Phys. Rev. E **55**, 3724 (1997).
- [39] L.P. Kadanoff and A.C. Brown, Ann. Phys. (N.Y.) **121**, 318 (1979).
- [40] M.P.M. den Nijs, J. Phys. A **12**, 1857 (1979).
- [41] S.-K. Yang, Nucl. Phys. B **285**, 183 (1987).
- [42] H. Saleur, J. Stat. Phys. **50**, 475 (1988).
- [43] M. Picco and R. Santachiara, J. Stat. Mech., P07027 (2010), [arXiv:1005.0493].
- [44] M. Picco and R. Santachiara, Critical interfaces and duality in the Ashkin–Teller model [arXiv:1011.1159].
- [45] R.J. Baxter, H.N.V. Temperley, and S.E. Ashley, Proc. Royal Soc. London A **358**, 535 (1978).
- [46] R.J. Baxter, Proc. Royal Soc. London A **383**, 43 (1982).
- [47] H. Saleur, Comm. Math. Phys. **132**, 657 (1990).

- [48] H. Saleur, Nucl. Phys. B **360**, 219 (1991).
- [49] J.L. Jacobsen and H. Saleur, Nucl. Phys. B **743**, 207 (2006) [arXiv:cond-mat/0512058].
- [50] J.-P. Lv, Y. Deng, and Q.-H. Chen, Phys. Rev E **84**, 021125 (2011), [arXiv:1009.3172].
- [51] H.N.V. Temperley and S.E. Ashley, Proc. Royal Soc. London A **365**, 371 (1979).
- [52] R.J. Baxter, J. Phys. A **19**, 2821 (1986).
- [53] R.J. Baxter, J. Phys. A **20**, 5241 (1987).
- [54] Y. Deng, T.M. Garoni, W. Guo, H.W.J. Blöte, and A.D. Sokal, Phys. Rev. Lett. **98**, 120601 (2007), [arXiv:cond-mat/0608447].
- [55] Q. Liu, Y. Deng, and T.M. Garoni, Nucl. Phys. B **846**, 283 (2011), [arXiv:1011.1980].
- [56] R.J. Baxter, Aust. J. Phys. **27**, 369 (1974).
- [57] R.J. Baxter, J. Math. Phys. **11**, 784 (1970).
- [58] C. Moore and M. E. J. Newman, J. Stat. Phys. **99**, 629 (2000), [arXiv:cond-mat/9902295].
- [59] R. Shrock R and S.-H. Tsai, J. Phys. A **30**, 495 (1997), [arXiv:cond-mat/9608095].
- [60] J. Salas, J. Phys. A **31**, 5969 (1998), [arXiv:cond-mat/9802145].
- [61] K. Kano and S. Naya, Progr. Theor. Phys. **10**, 158 (1953).